



Discovery of memantyl urea derivatives as potent soluble epoxide hydrolase inhibitors against lipopolysaccharide-induced sepsis



Fangyu Du ^a, Wenjiao Sun ^a, Christophe Morisseau ^b, Bruce D. Hammock ^b, Xuefei Bao ^{a, c}, Qiu Liu ^c, Chao Wang ^c, Tan Zhang ^c, Hao Yang ^c, Jun Zhou ^c, Wei Xiao ^{c, **}, Zhongbo Liu ^{d, ***}, Guoliang Chen ^{a, *}

^a Key Laboratory of Structure-Based Drug Design & Discovery of Ministry of Education, School of Pharmaceutical Engineering, Shenyang Pharmaceutical University, 103 Wenhua Road, Shenyang, Liaoning, 110016, China

^b Department of Entomology and Nematology and UC Davis Comprehensive Cancer Center, University of California Davis, One Shields Avenue, Davis, CA, 95616, USA

^c Jiangsu Kanion Pharmaceutical Co., Ltd., Jiangning Industrial City, Economic and Technological Development Zone, Lianyungang, Jiangsu, 222001, China

^d School of Pharmacy, Shenyang Pharmaceutical University, 103 Wenhua Road, Shenyang, Liaoning, 110016, China

ARTICLE INFO

Article history:

Received 29 January 2021

Received in revised form

18 June 2021

Accepted 25 June 2021

Available online 29 June 2021

Keywords:

Soluble epoxide hydrolase

Sepsis

Memantine derivatives

Cytokine storm

ABSTRACT

Sepsis, a systemic inflammatory response, caused by pathogenic factors including microorganisms, has high mortality and limited therapeutic approaches. Herein, a new soluble epoxide hydrolase (sEH) inhibitor series comprising a phenyl ring connected to a memantyl moiety via a urea or amide linkage has been designed. A preferential urea pharmacophore that improved the binding properties of the compounds was identified for those series via biochemical assay *in vitro* and *in vivo* studies. Molecular docking displayed that 3,5-dimethyl on the adamantyl group in **B401** could make van der Waals interactions with residues at a hydrophobic pocket of sEH active site, which might indirectly explain the subnanomolar level activities of memantyl urea derivatives *in vitro* better than **AR-9281**. Among them, compound **B401** significantly improved the inhibition potency with human and murine sEH IC₅₀ values as 0.4 nM and 0.5 nM, respectively. Although the median survival time of C57BL/6 mice in LPS-induced sepsis model was slightly increased, the survival rate did not reach significant efficacy. Based on safety profile, metabolic stability, pharmacokinetic and *in vivo* efficacy, **B401** demonstrated the proof of potential for this class of memantyl urea-based sEH inhibitors as therapeutic agents in sepsis.

© 2021 Elsevier Masson SAS. All rights reserved.

1. Introduction

Sepsis, also called cytokine storm or inflammation storm, a systemic inflammatory response caused by pathogenic factors including microorganisms, has high mortality and limited therapeutic approaches [1]. Epidemiological survey shows that global estimates of 31.5 million sepsis patients and 19.4 million severe sepsis cases and with potentially 5.3 million deaths every year [2]. Furthermore, the annual cost of hospital healthcare for severe sepsis patients in the U.S. is the highest among other diseases and

was around \$20 billion, which caused serious economic and psychological burden to patients [3]. The emerging of numerous pro-inflammatory cytokines in the progression of sepsis, has been identified [4]. Emerging evidence demonstrates that modulation of the innate immune response is an effective strategy to fight against infection caused by pathogenic microorganisms [5].

Coronavirus disease 2019 (COVID-19), caused by severe acute respiratory syndrome coronavirus 2 (SARS-CoV-2), characterized by systemic hyperinflammation associated with a life-threatening “cytokine storm” [6]. The pro-inflammatory cytokines levels including TNF- α , IL-6, IL-1 β , IL-1, IL-8, G-CSF, MCP-1, IP-10, and MIP-1 α in serum for patients with COVID-19 was significantly increased [7,8]. sEH inhibitors are effective not only in resolving pulmonary inflammation, but also in preventing pulmonary fibrosis [9–11], key hallmarks of COVID-19 that contribute to life-threatening complications such as acute respiratory distress syndrome

* Corresponding author.

** Corresponding author.

*** Corresponding author.

E-mail addresses: xw_kanion@163.com (W. Xiao), 546265581@qq.com (Z. Liu), chengguoliang@syphu.edu.cn (G. Chen).

(ARDS). It is reported that widely available corticosteroid such as dexamethasone can be applying for the treatment of cytokine storm, but corticosteroids only can be administered in lower dosage and short time because of their serious adverse effects [12,13]. Hence, there is an urgent need for new medicines for the treatment of sepsis in clinic.

Arachidonic acid (ARA), a 20-carbon polyunsaturated fatty acid (PUFA) derived from cell membrane phospholipid, which is largely biosynthesized into proinflammatory mediators by cyclooxygenase (COX) and lipoxygenase (LOX) pathways [14]. Both pathways have been pharmaceutically targeted, affording several pharmaceutical compounds (e.g., nonsteroidal anti-inflammatory drugs aspirin and blocking production with leukotriene inhibitor zileuton). Moreover, the ARA converted by CYP450 enzymes into epoxide metabolites epoxy-fatty acids (EpFAs) such as epoxyeicosatrienoic acids (EETs) which include regioisomers 5,6-EET, 8,9-EET, 11,12-EET and 14,15-EET [15]. Among them, 11,12-EET prevents the tumor necrosis factor (TNF)- α induced activation of NF- κ B and the subsequent increases in vascular cell adhesion molecule (VCAM)-1 expression in mice [16]. 14,15-EET also shows strongly anti-inflammatory effect [17]. EETs turn down production of inflammatory eicosanoids and cytokines through activating endoplasmic reticulum (ER) stress pathways, moving the ER stress response back toward maintaining homeostasis and inflammatory resolution [18]. However, the anti-inflammatory EETs are rapidly metabolized by the soluble epoxide hydrolase (sEH) to inactive or even proinflammatory diols [19]. Inhibition of sEH could stabilize and elevate EETs level, which have anti-inflammatory, anti-hypertensive, and analgesic properties, and also stimulates the production of pro-resolving mediators [20,21].

To date, three sEH inhibitors were moved into human clinical trials (Fig. 1). **AR-9281** by Arete Therapeutics was in phase II clinical trial for the treatment of hypertension and insulin resistance [22]. **GSK-2256294** by GlaxoSmithKline for the treatment of patients with chronic obstructive pulmonary disease (COPD) was investigated in several phase I clinical trials [23]. **EC-5026** by EicOsis for the management of neuropathic and inflammatory chronic pain was finished phase Ia clinical trial [24]. These data mean that the safety, efficacy and toxicological studies of sEH inhibitors have been substantially demonstrated in early preclinical investigation *in vivo* and *in vitro* as a class and the value of sEH as a target. Based on the significantly benefits of EETs or sEH inhibitors, we speculated that sEH is a potential target for the treatment of cytokine storm caused by SARS-CoV-2 or sepsis [25].

Structure-activity relationship (SAR) studies of sEH inhibitors revealed that ureas, amides, or carbamates group act as central primary pharmacophore, and attach to a relatively small group such as a phenyl, cyclohexyl and adamantyl on one side. On the other side could accommodate a large polar group termed the secondary pharmacophore, such as amide, carboxyl, ester, etc. [26,27] We report the discovery of a series of memantyl urea derivatives as potent sEH inhibitor and the identification of candidate **B401** for *in vivo* studies in lipopolysaccharide-induced sepsis model. The safety profile, metabolic stability, pharmacokinetic and *in vivo* efficacy associated with **B401** demonstrated the proof of

potential for this class of memantyl urea-based sEH inhibitors as therapeutic agents in sepsis.

2. Results and discussion

2.1. Design compounds

Our internal sEH inhibitor research program sought to identify small molecules that block the enzyme's catalytic function and therefore inhibit the formation of inactive or even proinflammatory diols. AR-9281 demonstrated impressive clinical response and has progressed to phase II trials. From the perspective of structure, it contained an amantadine group, leading to rapid cytochrome P450 based metabolism, and thus it has a short *in vivo* half-life [22]. Previous research revealed that piperine and piperlonguminine from *Scutellaria baicalensis* Georgi displayed significant inhibitory activity against sEH *in vitro*, with the IC₅₀ values at micromolar concentration [28,29]. On the other hand, comparing with amantadine (antiviral drugs), memantine (anti-Alzheimer disease), has good pharmacokinetic properties, with half-life ($t_{1/2}$) as 60 h [30]. Therefore, we supposed that introduction of memantyl group could increase half-life of target compounds. Meanwhile, we hypothesized that the introduction of 3,5-dimethyl at adamantyl group should increase hydrophobic interactions with sEH and afford some memantine derivatives. Taking into account for chemical character of memantine, and excellent inhibitory effects of memantyl urea derivatives, we replaced memantyl group with hydroxyl substituted adamantyl to obtain some hydroxyl substituted adamantyl urea derivatives as potent sEH inhibitors (Scheme 1). Although the adamantyl moiety of reported SAR of sEH inhibitors should be lipophilicity, molecular docking displayed OH-substituted adamantyl could make extra hydrogen bond with Gln384 of sEH protein (Fig. S1), which maybe further increase inhibitory effect on sEH.

2.2. Chemistry

The compounds in Table 1 were synthesized, as shown in Schemes 2 to 5. First, compounds **A101** to **A103** were synthesized in two steps from commercially available amines through succinic anhydride (**1**) acylation reaction. Then, commercially available memantine was then coupled to the acid intermediates **2–4** under standard amide coupling conditions (EDCI, HOBT, Et₃N, DCM) to give **A101 – A103** as shown in Scheme 2. Acids **6** to **8** were obtained using *cis*-butenedioic anhydride and amines as starting material. Interestingly, acid **6** was a *cis*-isomer, and *trans*-isomer product was not observed. The final compounds **A201 – A203** were obtained through an amide coupling condition reaction. The synthesis of **A301 – A303** began with the use of glutaric anhydride to transform the acid compounds **10–12**, then amide coupling to provide the title compounds.

As described in Scheme 3, the synthesis of compounds **A401 – A403** began with the halogenation reaction of 4-(methoxycarbonyl)benzoic acid (**13**) with thionyl chloride at 80 °C. The resulting methyl 4-(chlorocarbonyl)benzoate (**14**) was reacted

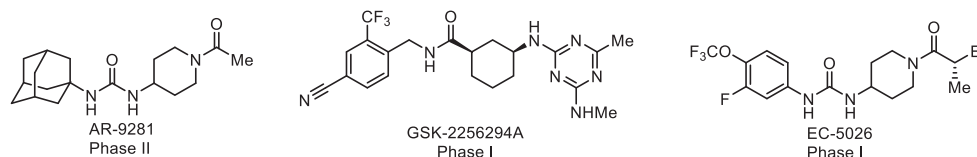
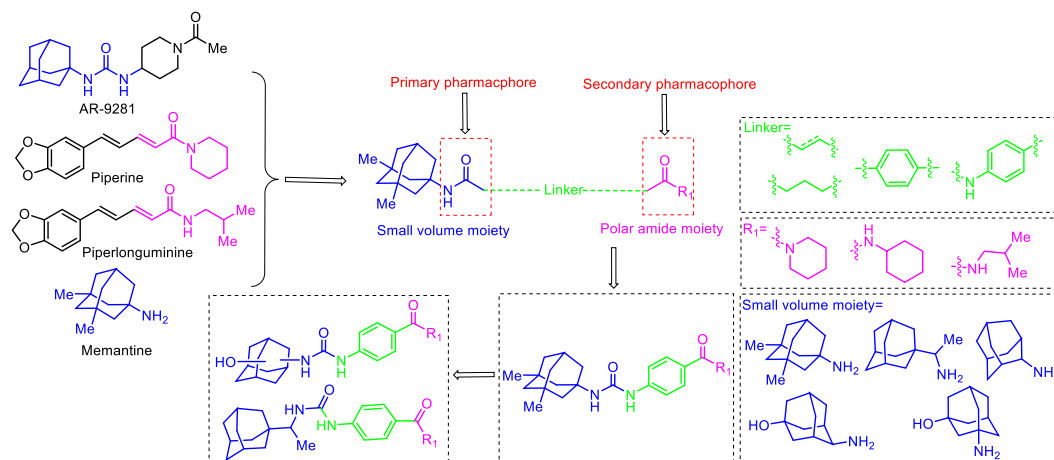


Fig. 1. Chemical structures of sEH inhibitors that moved into clinical trials.



Scheme 1. Schematic diagram depicting the procedure for the design of the target compounds.

with memantine to yield the ester **15**. Cleavage of the methyl ester moiety with LiOH at rt gave the free acid **16**, which coupled to the corresponding amines under standard amide coupling conditions to give **A401** – **A403**.

Commercially available rimantadine was respectively coupled to the acid intermediates **4** or **12** under standard amide coupling conditions (EDCI, HOBt, Et₃N, DCM) to give **C103** or **C303** as shown in Scheme 4. Compounds **D303** and **E303** were prepared *via* amide coupling reaction using 5-(isobutylamino)-5-oxopentanoic acid (**12**), 2-aminoadamantane (**18**) and 3-amino-1-hydroxyadamantane (**19**) as starting material.

Scheme 5 shows the synthetic pathways toward urea-based inhibitors. Acylation of amines with 4-nitrobenzoyl chloride **20** followed by the hydrogenation reduction of the nitro group in compounds **21**–**23** yielded the amino intermediates **24**–**26**. Then, the treatment with phenyl chloroformate in DCM yielded the key intermediates of carbamate **27**–**29** that was sufficiently stable to be isolated. Aminolysis of carbamates **27**–**29** with various adamantane derivatives (for example, memantine, rimantadine, 2-adamantanamine, *trans*-4-aminoadamantan-1-ol, 3-amino-1-adamantanol) afforded the urea-based compounds, as shown in Scheme 5.

2.3. Molecular docking

We used molecular modeling to predict possible binding mode of representative inhibitors (**B401** and **B402**) in the binding site of sEH (PDB code: 3WKE) using BIOVIA Discovery Studio 2016, as shown in Fig. 2. Generally, urea-group of compounds bound to the catalytic triad formed by Tyr383, Asp335 and Tyr466. Hydrophobic memantyl group bounds to the long branch formed by Trp336 and Gln384. Terminal benzamide moiety bounds to the short branch formed by Phe267, His524, Asp496 and Phe497. The carbonyl group of the urea makes a hydrogen bond to Tyr383, and the NH groups of the urea make two hydrogen bonds to Asp335 (Fig. 2B). The phenyl ring of **B401** binds in a hydrophobic pocket and makes π -cation interaction with His524. The methyl group at the 3-position of the memantyl sits in a hydrophobic cavity made up of Leu499 and Phe381. The methyl group at the 5-position of the memantyl sits in a hydrophobic pocket formed from the side chains of Met469 and phenyl ring of Tyr466. The terminal piperidinyl ring is deeply buried in a hydrophobic pocket and the body of the ring makes van der Waals contacts to the aliphatic portion of Val498 and His524. The compound **B402** contains a cyclohexylamino moiety and binds

in a similar mode as **B401**, as shown in Fig. 2D. Both compounds bind to sEH's active site primarily through hydrogen bond interactions by the urea moiety of the compounds (Fig. 2C).

2.4. sEH inhibition and Structure–Activity relationship

As the first step for the biological characterization of the amides, their potency as human sEH (HsEH) and murine sEH (MsEH) inhibitors was tested, as shown in Table 1. Compound **A302** was potent inhibitor of the MsEH (IC_{50} = 8.3 nM), while the compound was poor inhibitor of the human enzyme (IC_{50} = 1588.5 nM). Compounds **C103** and **E303** showed IC_{50} values on the human and murine sEH at nanomolar concentration (41.6 – 106.4 nM). Compounds featured by an amide moiety and attaching to memantyl were moderate inhibitors of the HsEH and MsEH at micromolar range. Different spacers (two-, three-carbon, and phenyl group) were used to evaluate the appropriate distance between the primary pharmacophore and the secondary pharmacophore. Results showed that the length of the spacer seem not to affect the inhibitory activity. For this reason, this set of derivatives was not further evaluated.

Taking into consideration of the availability of inhibitors with a urea as primary pharmacophore [24], then we have replaced the aliphatic amide with selected aniline scaffold, affording three memantyl urea-based inhibitors. Encouragingly, the *in vitro* screening process shown in Table 2 revealed three compounds (**B401** – **B403**) with adequate potency on HsEH and MsEH. The replacement of the terminal piperidine group with isobutylamine did not significantly impact the activity (**B401** vs **B403**). While the replacement of the terminal piperidine with a cyclohexylamine led to an obvious reduction (almost 6-fold) of the potency on human sEH (**B401** vs **B402**). Interestingly, compound **B402** did not reduce inhibitory effect on murine sEH with IC_{50} value of 0.4 nM. Molecular modeling showed that the surrounding of memantyl group has extra space volume which could accommodate the small substituents. Therefore, we decided to take rimantadyl moiety, connecting to urea group, since they would probe a very different chemical space compared with the memantyl group. However, the replacement of the memantyl moiety (**B401** – **B403**) with rimantadyl (**C401** – **C403**) gave different degrees of decrease in potency on both targets, suggesting that the position of adamantyl directly attached to urea group is important (Table 2). Among them, **C401** displayed moderate inhibitory potency with IC_{50} values of 3.9 nM and 2.4 nM on HsEH and MsEH.

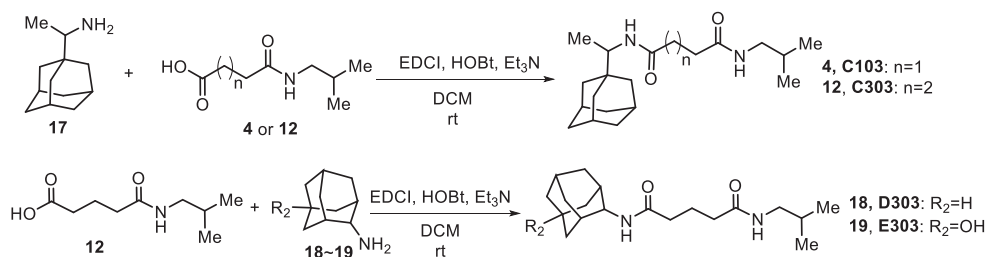
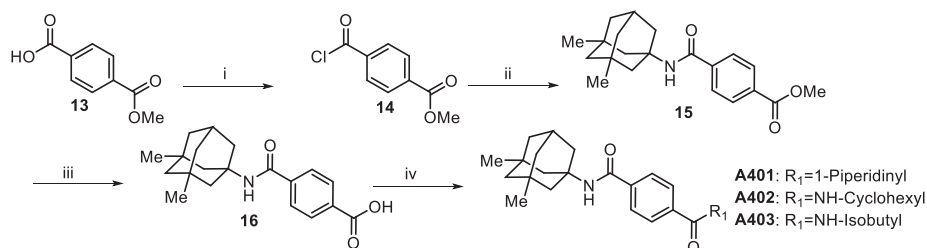
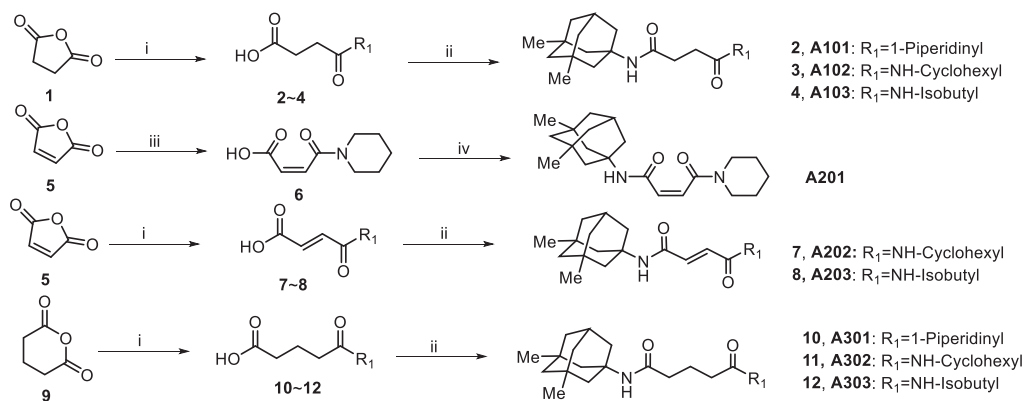
Table 1
Human (HsEH) and Murine (MsEH) sEH IC₅₀ of memantyl amide-based inhibitors ^a.

Comp.	Chemical Structure	HsEH IC ₅₀ (nM)	MsEH IC ₅₀ (nM)	cLogP ^b	LLE ^c
A101		2473.5	21686.6	2.48	3.13
A102		7891.7	179.7	3.21	1.89
A103		18915.9	4129.3	2.54	2.18
A201		21514.4	81198.4	2.87	1.79
A202		24440.6	5516.1	3.61	1.00
A203		9624.6	21120.3	2.94	2.07
A301		5930.8	5839.1	2.93	2.29
A302		1588.5	8.3	3.67	2.13
A303		6225.8	224.8	3.00	2.21
A401		26388.3	60713.1	3.92	0.65
A402		6287.8	1021.8	4.66	0.54
A403		>100000	6538.0	3.99	—
C303		7322.2	693.7	2.84	4.45
C103		50.8	43.5	3.30	1.84
D303		3581.8	2273.5	2.70	2.74
E303		41.6	106.4	1.49	5.89
AR-9281		13.8	1.7	1.30	6.57

^a IC₅₀ values are recorded on recombinant human sEH protein (HsEH) and murine sEH (MsEH) protein using PHOME as substrate at 50 μM concentration [31].^b The cLogP values were predicted by BIOVIA Discovery Studio 2016.^c Ligand lipophilicity efficiency (LLE) = pIC₅₀-cLogP [32].

Meanwhile, the substitution of 1-adamantyl group with 2-adamantyl group did not alter the inhibition properties (**D401** – **D403**) with the IC₅₀ values of subnanomolar levels, suggesting that the position is not critical for interaction with the sEH protein. We next introduced a hydroxyl group at C5 position (**E401** – **E403**) on the 2-adamantyl group with the expectation that lowering the compound lipophilicity should favorably impact the

in vitro activity. This change resulted in less active compounds in terms of the submicromolar potency. This effect might be attributed to an increased hydrophilic rather than an increased steric hindrance. Indeed, hydroxyl group at C3 position of adamantyl group (**F401** – **F403**) showed similar inhibitory activity. Although molecular docking displayed OH-substituted adamantyl could make extra hydrogen bond with Gln384 of sEH protein, regrettably,

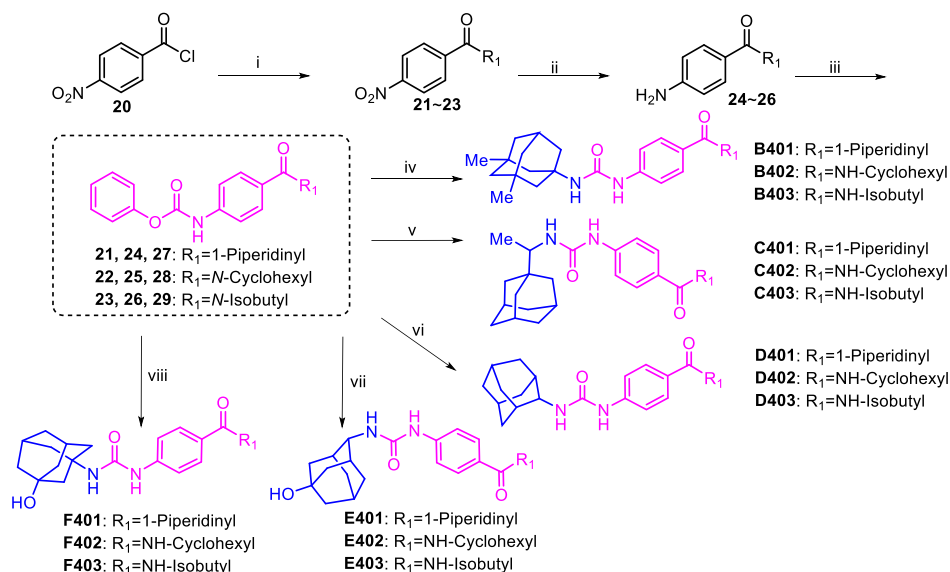


the inhibitory effect of these compounds didn't improve, and only retain some potency.

In addition, the cLogP values of all compounds were predicted by BIOVIA Discovery Studio 2016. In particular, a further calculation was conducted, affording ligand lipophilicity efficiency (LLE). Data in Table 2 showed that adding the hydroxyl group function at adamantane group not only significantly reduced inhibitory activity on both sEH protein but also reduced cLogP and LLE. By attaching memantyl or adamantyl group, cLogP values for the derivatives (especially B and C series compounds) are higher than memantine (cLogP = 3.82). The BBB penetration property of the representative compound **B401** was predicted by SwissADME [33]. The results revealed that those compounds showed favorable BBB permeability; therefore, the application of these compounds may be expanded to sepsis-associated encephalopathy which also could be related with sEH reactivity. Taken together, compounds **B401**, **B402**, **B403**, **D401**, **D402** and **D403** showed most promise as they displayed the highest LLE [34], which were selected for further studies.

2.5. In vivo safety

In order to determine the potential toxicological effect, acute toxicity tests were carried out in ICR (Institute of Cancer Research) mice (4 males, 4 females). The compounds were administered by intraperitoneal injection at single dose of 100 mg/kg, and advent events and symptoms were continuously observed for 14 days. No adverse effects were observed based on body weight as well as the absence of apparent behavior problems in compounds **B402** and **B403** groups, indicating that the two compounds are well tolerated (Supporting information Table S1, S2 and S3). Compared with the vehicle group, the average body weight gain of **D401** and **D403** groups were reduced. In addition, abnormal performance was observed based on eye secretion, indicating compounds **B401**, **D402**, **D403** and **AR-9281** displayed adverse effects, and fortunately abnormal performance of eye secretion is reversible (Supporting information Table S4). However, phase I study demonstrated that **AR-9281** was safe (dosage of 1200 mg/d) and well tolerated in



Scheme 5. Syntheses of urea-based compounds^a.

^aReactions and conditions: i) corresponding amines, Et₃N, THF, 0 °C to rt, 6 h; ii) H₂, 5%Pd–C, EtOH, 50 °C, 12 h; iii) K₂CO₃, phenyl chloroformate, DCM, 0 °C to rt, 7 h; iv) memantine, Et₃N, THF, reflux, 8 h; v) rimantadine, Et₃N, THF, reflux, 8 h; vi) 2-adamantanamine, Et₃N, THF, reflux, 8 h; vii) *trans*-4-aminoadamantan-1-ol, Et₃N, THF, reflux, 8 h; viii) 3-amino-1-adamantanol, Et₃N, THF, reflux, 8 h.

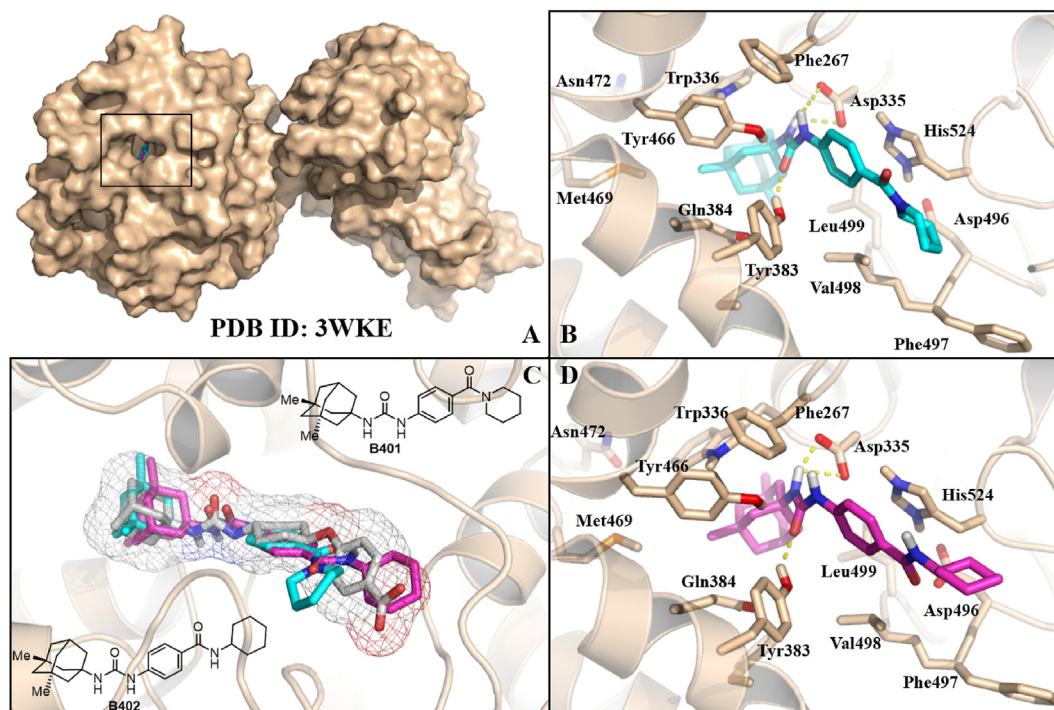


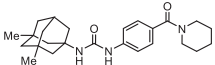
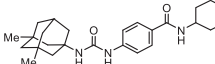
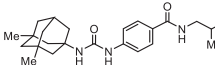
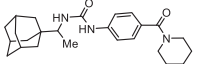
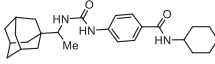
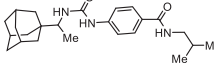
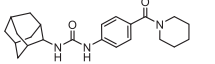
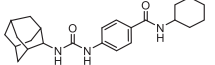
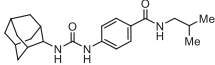
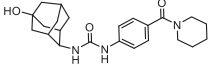
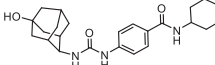
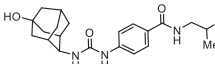
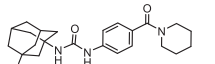
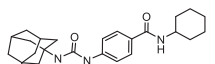
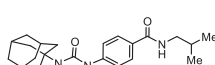
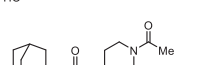
Fig. 2. Molecular modeling of sEH inhibitor bound to sEH (PDB code: 3WKE). A: Surface map of **B401** in blue and **B402** in pink bound to sEH in wheat; B: sEH in wheat bound to compound **B401** in blue. The carbonyl group of the urea makes a hydrogen bond to Tyr383, and the NH groups of the urea make two hydrogen bonds to Asp335. The phenyl ring of **B401** binds in a hydrophobic pocket and makes π -cation interaction with His524. C: Docked poses of **B401** (in blue) and **B402** (in pink) overlaid over X-ray pose of native ligand (in white) presenting the surface of sEH binding pocket. Three compounds bind to sEH's active site primarily through hydrogen bond interactions by the urea moiety of the compounds. D: sEH in wheat bound to compound **B402** in pink. The carbonyl group of the urea makes a hydrogen bond to Tyr383, and the NH groups of the urea make two hydrogen bonds with Asp335. The phenyl ring of **B401** binds in a hydrophobic pocket and makes π -cation interaction with His524.

healthy volunteers [22]. Noteworthy, this adverse effect presented gender differences, among male mouse appearing to this performance. The observed efficacy and safety profile associated with these compounds demonstrated the proof of concept for this class of memantyl urea-based sEH inhibitors as therapeutic agents in related diseases.

2.6. Microsomal stability

The microsomal stability of **B401** was evaluated in human and rat liver microsomes, which are widely used to determine the likely degree of primary metabolic clearance in the liver. As shown in Table 3, the *in vitro* metabolism of **B401** remained in both human

Table 2
Human (HsEH) and Murine (MsEH) sEH IC₅₀ of urea-based inhibitors^a.

Comp.	Structure	HsEH IC ₅₀ (nM)	MsEH IC ₅₀ (nM)	cLogP ^b	LLE ^c
B401		0.4	0.5	3.83	5.57
B402		2.3	0.4	4.57	4.07
B403		0.7	0.4	3.90	5.25
C401		3.9	2.4	4.13	4.28
C402		217.2	13.7	4.86	1.80
C403		59.8	28.8	4.20	3.03
D401		0.4	0.4	3.53	5.86
D402		1.4	0.4	4.27	4.58
D403		0.9	0.4	3.60	5.44
E401		216.8	496.6	2.32	4.35
E402		493.0	462.6	3.05	3.25
E403		248.9	2348.6	2.39	4.22
F401		120.4	88.8	2.08	4.84
F402		795.6	94.2	2.82	3.28
F403		949.1	290.6	2.15	3.87
AR-9281		13.8	1.7	1.30	6.57

^a IC₅₀ values are recorded on recombinant human sEH protein (HsEH) and murine sEH (MsEH) protein using PHOME as substrate at 50 μM concentration.³¹

^b The cLogP values were predicted by BIOVIA Discovery Studio 2016.

^c Ligand lipophilicity efficiency (LLE) = pIC₅₀-cLogP.³²

and rat liver microsomes, with half-lives of 25 and 31 min, respectively.

2.7. Pharmacokinetic study of B401

To identify the optimal candidate for evaluation *in vivo*, the pharmacokinetics profile of **B401** was determined with a single

Table 3

Mean of concentrations of **B401** in microsomal buffer at different time (ng/mL).

Time (min)	0	5	10	20	30	60	t _{1/2} (min)
Human	100.0	58.91	42.97	26.38	17.15	12.42	25.37
Rat	100.0	17.70	15.48	9.33	6.04	5.27	30.94

dose of 30 mg/kg by oral (*po*) and a single dose of 3 mg/kg by intravenous (*iv*) administration in the Sprague Dawley (SD) rats. Pharmacokinetic parameters are shown in Table 4. After oral administration blood levels were detected up to 24 h. The maximum total concentration of **B401** (0.33 μ M) was reached after 1.36 h; total exposure area under the curve AUC_{0-24} was 1.304 μ M·h. Poor exposures of compound **B401** were obtained, indicating bioavailability of 7.1%. The pharmacokinetic properties revealed compound **B401** has a plasma half-life ($t_{1/2}$) of 2.24 h.

According to pharmacokinetic parameters, compound **B401** displayed large apparent volume of distribution (V_d), which indicated that compound **B401** could be highly bound to plasma protein. Therefore, the percentage plasma protein binding (%PPB) of mice was determined using equilibrium dialysis method. The result of this screen demonstrated that compound **B401** exhibited high % PPB (98.6%) value. The high %PPB can be partly attributed to the presence of the memantyl urea and benzamide moieties, as plasma protein binding interactions are hydrophobic in nature.

2.8. In Vivo Efficacy

To determine if the administration of compound **B401** to C57BL/6 mice would produce a survival benefit (an increase in the median survival time), *in vivo* efficacy was further evaluated in lipopolysaccharide (LPS) induced sepsis model, and compound **B401** was then designed with three doses of 1, 5 and 20 mg/kg, as shown in Table 5. The numbers in parentheses indicated the number of surviving mice.

The cumulative deaths of vehicle group at 24 h was 4, and the survival rate was 71.4%. The survival rate within 72 h was 28.6%, and the median survival time was 31.2 h. Adrenocortical steroid dexamethasone significantly improved survival rate (100%) vs vehicle (28.6%). Mice treated with **B401** at doses of 1 mg/kg and 5 mg/kg couldn't improve survival rate and median survival time. The both cumulative deaths at 24 h were 6. The median survival was 31.7 and 25.8, respectively. Mice treated with higher dose **B401** (20 mg/kg) showed increased survival, with a median survival rate of 53.8 h compared with 31.2 h for the vehicle mice. The cumulative deaths at 24 h were 3, survival rate of 24 h and 72 h were 78.6 and 35.7, respectively. (Fig. 3). Considering the compound **B401** is highly bound to mouse plasma proteins, the amount of drug available to reach the target is reduced. Subsequently, the efficacy of compound **B401** may be significantly reduced. Despite not reaching significant efficacy, the ability to provide a survival advantage in this LPS-induced sepsis model illustrates the potential of **B401** as a lead compound for the further optimization.

3. Conclusion

A novel series of memantyl based sEH inhibitors was created from an initial **AR-9281**, memantine, piperine and piperlongumine *via* molecular hybridization, bioisosterism and computer aided drug design. The ligand lipophilicity efficiency (LLE) and potency of the initial compounds were improved considerably during the course of these optimization activities. These efforts culminated with the identification of an optimized molecule, compound **B401**, which exhibited potent *in vitro* enzyme activity in subnanomolar

level, and increased the median survival time of C57BL/6 mice in LPS-induced sepsis model. Despite survival rate did not reach significant efficacy vs vehicle, based on safety profile, metabolic stability, pharmacokinetic and *in vivo* efficacy, compound **B401** demonstrated the proof of potential for this class of memantyl urea-based sEH inhibitors as therapeutic agents in sepsis. Considering the drug efficacy *in vivo* is determined by the concentration of free drug, rather than the total concentration in plasma; therefore, this moderate efficacy could be partly attributed to the high %PPB (98.6%). Further optimization of the pharmaceutical properties of this class of compounds and evaluation on combination with dexamethasone to decrease the dosage of dexamethasone will be reported in due course.

4. Experimental section

4.1. General information

Unless otherwise stated, solvents and all commercially available reagents were used directly without further purification. Melting points were measured with an X-4 melting point apparatus and were uncorrected. ^1H NMR spectra were recorded on an Ascent 400 MHz spectrometer using Me_4Si (TMS) as the internal standard. Electrospray ionization (ESI) mass spectra was recorded using an 1100 Series MSD Trap SL. High-resolution mass spectrometry (HRMS) results were recorded using an Agilent Technologies 6530 Accurate-Mass Q-TOF MS. The reactions were monitored by thin-layer chromatography (TLC, HG/T2354–92, GF254), and terminated as judged by the consumption of starting material.

4.2. Chemistry

General procedure for acylation of anhydrides with amines. Amines (50.0 mmol) was added dropwise to a solution of anhydrides (50.0 mmol) in dichloromethane (30 mL) at 0 °C. The reaction mixture was allowed to warm to rt and stirred for 2 h. Then solvent was evaporated, and the crude product was purified by recrystallization in EtOAc to obtain the title compound as white solid.

General procedure for acylation of carboxylic acids with amines. To a solution of EDCI (0.78 g, 4.05 mmol), HOBT (0.36 g, 4.05 mmol), Et_3N (1.36 g, 13.50 mmol) in dry DCM (20 mL) was added carboxylic acids derivatives (2.70 mmol) at rt and stirred for 30 min. Then, corresponding amines or amines hydrochloride (2.70 mmol) was added. The mixture was stirred at rt for 4 h. Then, the reaction mixture was poured into water (20 mL). The resulting mixture was extracted with DCM (20 mL \times 3). The combined organic layers were washed twice with saturated NaHCO_3 aqueous (20 mL), once with water (20 mL) and once with brine (20 mL). The separated organic layer was dried with MgSO_4 , filtered, and concentrated under vacuum produce crude product, which was purified by recrystallization in acetone to obtain the title compound as a white solid.

Compounds **A101** – **A303** were synthesized *via* two steps according to general procedure for acylation of anhydrides with amines and carboxylic acids with amines.

*N-((1*r*,3*R*,5*S*,7*r*)-3,5-dimethyladamantan-1-yl)-4-oxo-4-*

Table 4

Pharmacokinetics of **B401** in rats following intravenous and oral administration ($n = 6$).

Route	T_{max} (h)	C_{max} (μ M)	$t_{1/2}$ (h)	CL (L/h/kg)	V_z (L/kg)	$AUC_{(0-24)}$ (μ M·h)	$AUC_{(0-\infty)}$ (μ M·h)	Bioavailability (%)
<i>iv</i> (3 mg/kg)	0.64	3.64	1.23	4.30	7.83	1.834	1.835	
<i>po</i> (30 mg/kg)	1.36	0.33	2.24	269.79	1097.80	1.304	1.305	7.1

Table 5

Survival rate of 24 h and 72 h (n = 14).

Vehicle	B401 (1 mg/kg)	B401 (5 mg/kg)	B401 (20 mg/kg)	Dexamethasone (5 mg/kg)
Median survival/h	31.2	31.7	25.8	53.8
Survival rate % (24 h)	71.4 (10)	57.1 (8)	57.1 (8)	78.6 (11)
Survival rate % (72 h)	28.6 (4)	21.4 (3)	7.1 (1)	35.7 (5)
				100 (14)

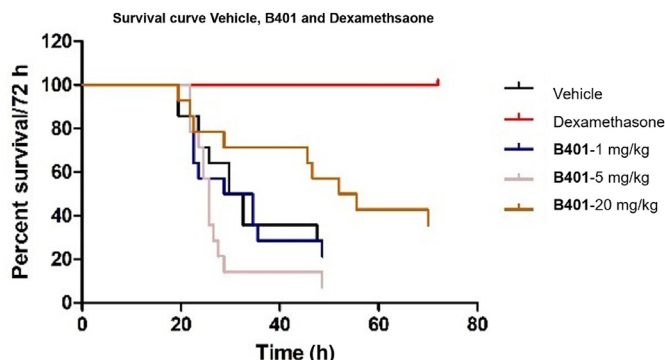


Fig. 3. Increased survival of C57BL/6 mice in LPS-induced sepsis following **B401** treatment. Mice treated with 20 mg/kg **B401** by intraperitoneal injection (ip) (wheat, n = 14) exhibited a survival advantage compared to mice treated with soybean oil vehicle (black, n = 14).

(piperidin-1-yl)butanamide (**A101**). White solid (0.50 g, 53%). m.p. 102–103 °C. ^1H NMR (400 Hz, CDCl_3) δ (ppm) 3.55 (t, J = 5.2 Hz, 2H), 3.42 (t, J = 4.9 Hz, 2H), 2.65 (t, J = 6.6 Hz, 2H), 2.53 (br, 2H), 2.14–2.11 (m, 1H), 1.83 (d, J = 2.4 Hz, 2H), 1.68–1.62 (m, 6H), 1.58–1.51 (m, 4H), 1.39–1.35 (m, 2H), 1.29–1.26 (m, 2H), 1.20–1.15 (m, 1H), 1.13–1.10 (m, 1H), 0.84 (s, 6H). ^{13}C NMR (100 Hz, CDCl_3) δ (ppm) 171.7, 170.1, 53.3, 50.6, 47.5, 46.5, 42.9, 42.7, 40.1, 32.7, 32.3, 30.1, 30.0, 28.8, 26.4, 25.6, 24.5. ESI-MS m/z : 347.3 $[\text{M}+\text{H}]^+$.

N [1]-cyclohexyl-*N* [4]-((1*r*,3*R*,5*S*,7*r*)-3,5-dimethyladamantan-1-yl)succinimide (**A102**). White solid (0.38 g, 39%). m.p. 128–130 °C. ^1H NMR (400 Hz, CDCl_3) δ (ppm) 5.88 (br, 1H), 5.67 (br, 1H), 3.78–3.68 (m, 1H), 2.46 (br, 4H), 2.15–2.12 (m, 1H), 1.90–1.86 (m, 2H), 1.82 (d, J = 2.3 Hz, 2H), 1.72–1.66 (m, 2H), 1.63 (br, 4H), 1.60–1.58 (m, 1H), 1.39–1.33 (m, 4H), 1.30–1.26 (m, 3H), 1.21–1.20 (m, 1H), 1.19–1.10 (m, 4H), 1.84 (s, 6H). ^{13}C NMR (100 Hz, CDCl_3) δ (ppm) 171.4, 171.3, 53.5, 50.6, 48.2, 47.5, 42.7, 40.1, 33.2, 33.0, 32.3, 32.2, 30.1, 30.0, 25.5, 24.8. ESI-MS m/z : 361.3 $[\text{M}+\text{H}]^+$.

N [1]-((1*r*,3*R*,5*S*,7*r*)-3,5-dimethyladamantan-1-yl)-*N* [4]-isobutylsuccinamide (**A103**). White solid (0.40 g, 44%). m.p. 123–125 °C. ^1H NMR (400 Hz, CDCl_3) δ (ppm) 6.16 (br 1H), 5.60 (br, 1H), 3.06 (q, J = 6.7 Hz, 2H), 2.50–2.44 (m, 4H), 2.14–2.11 (m, 1H), 1.80 (d, J = 2.7 Hz, 2H), 1.79–1.72 (m, 1H), 1.62 (s, 4H), 1.38–1.35 (m, 2H), 1.29–1.26 (m, 2H), 1.19–1.14 (m, 2H), 0.91 (s, 3H), 0.90 (s, 3H), 0.84 (s, 6H). ^{13}C NMR (100 Hz, CDCl_3) δ (ppm) 172.4, 171.4, 53.5, 50.6, 47.5, 46.9, 42.7, 40.1, 33.1, 32.3, 32.1, 30.1, 30.0, 28.5, 20.1. ESI-MS m/z : 355.3 $[\text{M}+\text{Na}]^+$.

(*Z*)-*N*-((1*r*,3*R*,5*S*,7*r*)-3,5-dimethyladamantan-1-yl)-4-oxo-4-(piperidin-1-yl)but-2-enamide (**A201**). White solid (0.10 g, 11%). m.p. 162–164 °C. ^1H NMR (400 Hz, CDCl_3) δ (ppm) 7.35 (br, 1H), 6.26 (d, J = 12.9 Hz, 1H), 5.97 (d, J = 12.5 Hz, 1H), 3.61 (t, J = 5.6 Hz, 2H), 3.42 (t, J = 5.5 Hz, 2H), 2.15–2.12 (m, 1H), 1.85 (d, J = 2.0 Hz, 2H), 1.70–1.54 (m, 10H), 1.40–1.37 (m, 2H), 1.29–1.26 (m, 2H), 1.20–1.10 (m, 2H), 0.85 (s, 6H). ^{13}C NMR (100 Hz, CDCl_3) δ (ppm) 165.7, 164.2, 132.1, 128.6, 53.7, 50.7, 47.7, 47.3, 42.7, 42.5, 39.9, 32.3, 30.1, 26.4, 25.5, 24.4. ESI-MS m/z : 345.3 $[\text{M}+\text{H}]^+$.

N [1]-cyclohexyl-*N* [4]-((1*r*,3*R*,5*S*,7*r*)-3,5-dimethyladamantan-1-yl)fumaramide (**A202**). White solid (0.33 g, 34%). m.p.

234–236 °C. ^1H NMR (400 Hz, CDCl_3) δ (ppm) 6.84 (d, J = 14.8 Hz, 1H), 6.76 (d, J = 14.8 Hz, 1H), 5.81 (d, J = 7.6 Hz, 1H), 5.72 (br, 1H), 3.89–3.81 (m, 1H), 2.18–2.14 (m, 1H), 1.96–1.92 (m, 2H), 1.87 (d, J = 2.7 Hz, 2H), 1.76–1.69 (m, 6H), 1.65–1.60 (m, 1H), 1.43–1.29 (m, 6H), 1.23–1.13 (m, 5H), 0.86 (s, 6H). ^{13}C NMR (100 Hz, CDCl_3) δ (ppm) 163.5, 134.7, 132.6, 54.1, 50.6, 48.6, 47.3, 42.6, 40.1, 33.0, 32.4, 30.1, 30.0, 25.5, 24.9. ESI MS m/z : 359.3 $[\text{M}+\text{H}]^+$.

N [1]-((1*r*,3*R*,5*S*,7*r*)-3,5-dimethyladamantan-1-yl)-*N* [4]-isobutylfumaramide (**A203**). White solid (0.33 g, 36%). m.p. 97–99 °C. ^1H NMR (400 Hz, CDCl_3) δ (ppm) 7.36 (br, 1H), 6.03 (d, J = 14.0 Hz, 1H), 6.01 (q, J = 14.0 Hz, 1H), 3.15 (t, J = 5.7 Hz, 2H), 2.7–2.15 (m, 1H), 1.89 (br, 2H), 1.73–1.68 (m, 2H), 1.65–1.63 (m, 1H), 1.42–1.39 (m, 2H), 1.32–1.29 (m, 2H), 1.28–1.24 (m, 2H), 1.21–1.13 (m, 2H), 0.96 (s, 3H), 0.95 (s, 3H), 0.86 (s, 6H). ^{13}C NMR (100 Hz, CDCl_3) δ (ppm) 165.1, 164.3, 133.5, 132.3, 54.1, 50.6, 47.2, 47.1, 42.7, 39.7, 32.4, 30.1, 29.7, 28.3, 20.2. ESI MS m/z : 333.3 $[\text{M}+\text{H}]^+$.

N-((1*r*,3*R*,5*S*,7*r*)-3,5-dimethyladamantan-1-yl)-5-oxo-5-(piperidin-1-yl)pentanamide (**A301**). White solid (0.34 g, 35%). m.p. 98–100 °C. ^1H NMR (400 Hz, CDCl_3) δ (ppm) 5.65 (br, 1H), 3.54 (t, J = 5.4 Hz, 2H), 3.40 (t, J = 5.4 Hz, 2H), 2.40 (t, J = 7.0 Hz, 2H), 2.18 (t, J = 7.1 Hz, 2H), 2.14–2.11 (m, 1H), 1.67–1.62 (m, 6H), 1.58–1.52 (m, 4H), 1.40–1.35 (m, 2H), 1.29–1.26 (m, 2H), 1.20–1.10 (m, 2H), 0.84 (s, 6H). ^{13}C NMR (100 Hz, CDCl_3) δ (ppm) 171.9, 170.9, 53.4, 50.6, 47.6, 46.7, 42.7, 42.6, 40.2, 36.7, 32.4, 32.1, 30.1, 30.0, 26.6, 25.6, 24.5, 21.6. ESI MS m/z : 361.3 $[\text{M}+\text{H}]^+$.

N [1]-cyclohexyl-*N* [5]-((1*r*,3*R*,5*S*,7*r*)-3,5-dimethyladamantan-1-yl)glutaramide (**A302**). White solid (0.35 g, 34%). m.p. 155–157 °C. ^1H NMR (400 Hz, CDCl_3) δ (ppm) 5.72 (s, 1H), 5.51 (br, 1H), 3.80–3.71 (m, 1H), 2.23 (t, J = 7.1 Hz, 2H), 2.17 (t, J = 7.0 Hz, 2H), 2.14–2.12 (m, 1H), 1.94–1.87 (m, 4H), 1.82 (d, J = 2.5 Hz, 2H), 1.73–1.67 (m, 2H), 1.64 (s, 4H), 1.61–1.60 (m, 1H), 1.41–1.34 (m, 4H), 1.32–1.27 (m, 2H), 1.22–1.09 (m, 5H), 0.85 (s, 6H). ^{13}C NMR (100 Hz, CDCl_3) δ (ppm) 171.9, 171.7, 53.5, 50.6, 48.1, 47.6, 42.7, 40.2, 36.3, 35.6, 33.2, 32.4, 33.2, 32.4, 30.1, 30.0, 25.5, 24.9, 22.3. ESI-MS m/z : 375.4 $[\text{M}+\text{H}]^+$.

N [1]-((1*r*,3*R*,5*S*,7*r*)-3,5-dimethyladamantan-1-yl)-*N* [5]-isobutylglutaramide (**A303**). White solid (0.39 g, 41%). m.p. 130–132 °C. ^1H NMR (400 Hz, CDCl_3) δ (ppm) 5.86 (br, 1H), 5.45 (br, 1H), 3.07 (dd, J = 6.7 Hz, 6.1 Hz, 2H), 2.27 (t, J = 7.1 Hz, 2H), 2.17 (t, J = 7.4 Hz, 2H), 2.14–2.12 (m, 1H), 1.95–1.88 (m, 2H), 1.82 (d, J = 2.9 Hz, 2H), 1.80–1.73 (m, 1H), 1.64 (s, 4H), 1.39–1.36 (m, 2H), 1.30–1.27 (m, 2H), 1.20–1.11 (m, 2H), 0.92 (s, 3H), 0.91 (s, 3H), 0.85 (s, 6H). ^{13}C NMR (100 Hz, CDCl_3) δ (ppm) 172.7, 171.9, 53.5, 50.6, 47.6, 46.9, 42.7, 40.2, 36.3, 35.4, 32.4, 30.1, 30.0, 28.5, 22.3, 20.1. ESI MS m/z : 349.3 $[\text{M}+\text{H}]^+$.

Methyl 4-(chlorocarbonyl)benzoate (**14**). A mixture of 4-(methoxycarbonyl)benzoic acid **13** (18.0 g, 100.0 mmol) and DMF (0.5 mL) in SOCl_2 (75 mL) was heated to reflux for 2 h. After cooling to r.t., the reaction mixture was concentrated *in vacuo* to obtain. After cooling to rt, the reaction mixture was concentrated *in vacuo* to obtain methyl 4-(chlorocarbonyl)benzoate **14** as a light yellow solid. It was used in the following reaction without any further purification.

Methyl 4-(((1*r*,3*R*,5*S*,7*r*)-3,5-dimethyladamantan-1-yl)carbamoyl)benzoate (**15**). To a solution of Et_3N (12.6 g, 0.13 mol), DMAP (0.56 g, 5.0 mmol) in dry DCM (30 mL) was added menantine

hydrochloride (5.40 g, 25.0 mmol). To the reaction mixture was added dropwise solution of **14** (9.90 g, 50.0 mmol) in dry DCM (30 mL) at 0 °C. The resulting mixture was allowed to warm to rt and stirred for 8 h. The reaction mixture was poured into water (40 mL), extracted with DCM (30 mL × 3). The combined organic layers were washed with saturated NaHCO₃ aqueous (30 mL × 2), once with water (30 mL) and once with brine (30 mL). The separated organic layer was dried with MgSO₄, filtered, and concentrated under vacuum produce crude **15** as a white solid (4.80 g, 80%). It was used in the following reaction without any further purification.

4-(((1*r*,3*R*,5*S*,7*r*)-3,5-Dimethyladamantan-1-yl)carbamoyl)benzoic acid (**16**). Crude **15** (1.0 g, 2.93 mmol) was dissolved in THF (10 mL), followed by the addition of H₂O (7 mL) and LiOH·H₂O (0.37 g, 8.79 mmol) at rt. After 3 h, the reaction was filtered and concentrated under vacuum. To the residues was added H₂O (20 mL), after cooling to 0 °C, the pH was adjusted to 1 using 2 N HCl. The resulting precipitation was filtered and washed with H₂O to give a white solid (0.90 g, 94%).

General procedure for the syntheses of A401 –A403. To a solution of EDCI (0.26 g, 1.38 mmol), HOBT (0.19 g, 1.38 mmol), Et₃N (0.46 g, 4.55 mmol) in dry DCM (20 mL) was added **16** (0.30 g, 0.92 mmol) at rt and stirred for 30 min. Then, corresponding amines (1.10 mmol) was added. The mixture was stirred at rt for 24 h. Then, the reaction mixture was poured into water (20 mL). The resulting mixture was extracted with DCM (20 mL × 3). The combined organic layers were washed once with water (20 mL) and once with brine (20 mL). The separated organic layer was dried with MgSO₄, filtered, and concentrated under vacuum to produce crude product, which was purified by column chromatography on silica gel to obtain a white solid.

N-((1*r*,3*R*,5*S*,7*r*)-3,5-Dimethyladamantan-1-yl)-4-(piperidine-1-carbonyl)benzamide (**A401**). White solid (0.20 g, 56%). m.p. 148–150 °C. ¹H NMR (400 Hz, CDCl₃) δ (ppm) 7.73 (d, *J* = 8.2 Hz, 2H), 7.42 (d, *J* = 8.2 Hz, 2H), 5.83 (s, 1H), 3.68 (br, 2H), 3.31 (br, 2H), 2.21–2.18 (m, 1H), 1.96 (d, *J* = 2.2 Hz, 2H), 1.81–1.73 (m, 4H), 1.67 (br, 6H), 1.45–1.32 (m, 4H), 1.26–1.16 (m, 2H), 0.59 (s, 6H). ¹³C NMR (100 Hz, CDCl₃) δ (ppm) 169.4, 166.0, 139.0, 136.8, 126.93, 126.91, 54.1, 50.6, 47.6, 42.7, 40.2, 32.5, 30.2, 30.1, 24.5. ESI-HRMS: *m/z* [M+Na]⁺ calcd for C₂₅H₃₄N₂O₂Na: 417.2512; found: 417.2543.

N [1]-cyclohexyl-*N* [4]-((1*r*,3*R*,5*S*,7*r*)-3,5-dimethyladamantan-1-yl)terephthalamide (**A402**). White solid (0.21 g, 57%). m.p. 257–259 °C. ¹H NMR (400 Hz, CDCl₃) δ (ppm) 7.76 (q, *J* = 14.6, 8.7 Hz, 4H), 6.00 (d, *J* = 7.9 Hz, 1H), 5.84 (s, 1H), 2.21–2.19 (m, 1H), 2.06–2.02 (m, 2H), 1.97 (d, *J* = 2.0 Hz, 2H), 1.81–1.75 (m, 6H), 1.69–1.64 (m, 1H), 1.48–1.30 (m, 6H), 1.28–1.17 (m, 5H), 0.89 (s, 6H). ¹³C NMR (100 Hz, CDCl₃) δ (ppm) 165.8, 138.4, 137.3, 127.1, 126.9, 54.2, 50.6, 48.9, 47.6, 42.7, 40.2, 33.2, 32.5, 30.2, 30.1, 25.6, 24.9. ESI-HRMS: *m/z* [M+Na]⁺ calcd for C₂₆H₃₆N₂O₂Na: 431.2669; found: 431.2697.

N [1]-((1*r*,3*R*,5*S*,7*r*)-3,5-dimethyladamantan-1-yl)-*N* [4]-isobutylterephthalamide (**A403**). White solid (0.21 g, 60%). m.p. 234–236 °C. ¹H NMR (400 Hz, CDCl₃) δ (ppm) 7.76 (q, *J* = 16.7, 8.1 Hz, 4H), 6.22 (br, 1H), 5.85 (br, 1H), 3.30 (t, *J* = 6.2 Hz, 2H), 2.21–2.19 (m, 1H), 1.97 (d, *J* = 2.2 Hz, 2H), 1.95–1.88 (m, 1H), 1.82–1.74 (m, 4H), 1.46–1.32 (m, 4H), 1.26–1.17 (m, 2H), 0.99 (s, 3H), 0.98 (s, 3H), 0.89 (s, 6H). ¹³C NMR (100 Hz, CDCl₃) δ (ppm) 166.8, 165.9, 138.4, 137.2, 127.1, 127.0, 54.2, 50.6, 47.6, 47.5, 42.7, 40.2, 32.5, 30.2, 30.1, 29.7, 28.6, 20.2. ESI-HRMS: *m/z* [M+Na]⁺ calcd for C₂₄H₃₄N₂O₂Na: 405.2512; found: 405.2533.

N [1]-((1*r*,3*R*,5*S*,7*r*)-adamantan-1-yl)ethyl)-*N* [4]-isobutylsuccinamide (**C103**). According to General procedure for acylation of carboxylic acids with amines. **C103** was obtained as a white solid (0.38 g, 42%). m.p. 186–188 °C. ¹H NMR (400 Hz, CDCl₃) δ (ppm) 6.24 (br, 1H), 5.94 (br, 1H), 3.71–3.63 (m, 1H), 3.13–3.00 (m,

2H), 2.60–2.49 (m, 4H), 1.97 (br, 3H), 1.80–1.74 (m, 1H), 1.72–1.60 (m, 6H), 1.54–1.45 (m, 6H), 1.00 (d, *J* = 6.9 Hz, 3H), 0.90 (d, *J* = 6.7 Hz, 6H). ¹³C NMR (100 Hz, CDCl₃) δ (ppm) 172.3, 171.7, 53.1, 47.0, 38.3, 37.0, 35.7, 32.4, 32.2, 28.5, 28.3, 20.1, 14.5. ESI-HRMS: *m/z* [M+Na]⁺ calcd for C₂₀H₃₄N₂O₂Na: 357.2512; found: 357.2529.

N [1]-((1*r*,3*R*,5*S*,7*r*)-adamantan-1-yl)ethyl)-*N* [5]-isobutylglutaramide (**C303**). According to General procedure for acylation of carboxylic acids with amines. **C303** was obtained as a white solid as a white solid (0.44 g, 46%). m.p. 191–193 °C. ¹H NMR (400 Hz, CDCl₃) δ (ppm) 5.95 (br, 1H), 5.66 (br, 1H), 3.74–3.67 (m, 1H), 3.08 (t, *J* = 6.6 Hz, 2H), 2.31–2.27 (m, 4H), 2.00–1.94 (m, 5H), 1.82–1.74 (m, 1H), 1.72–1.60 (m, 6H), 1.55–1.46 (m, 6H), 1.01 (d, *J* = 6.9 Hz, 3H), 0.92 (d, *J* = 6.7 Hz, 6H). ¹³C NMR (100 Hz, CDCl₃) δ (ppm) 172.6, 171.9, 52.9, 46.9, 38.4, 37.0, 35.7, 35.5, 28.5, 28.3, 22.4, 20.1, 14.6. ESI-HRMS: *m/z* [M+Na]⁺ calcd for C₂₁H₃₆N₂O₂Na: 371.2669; found: 371.2684.

N [1]-((1*S*,2*R*,5*R*)-adamantan-2-yl)-*N* [5]-isobutylglutaramide (**D303**). According to General procedure for acylation of carboxylic acids with amines. **D103** was obtained as a white solid (0.44 g, 51%). m.p. 186–188 °C. ¹H NMR (400 Hz, DMSO-*d*₆) δ (ppm) 7.74 (t, *J* = 5.4 Hz, 1H), 7.64 (t, *J* = 7.5 Hz, 2H), 3.83 (d, *J* = 7.3 Hz, 1H), 2.85 (t, *J* = 6.2 Hz, 2H), 2.13 (t, *J* = 7.4 Hz, 2H), 2.06 (t, *J* = 7.4 Hz, 2H), 1.99–1.95 (m, 2H), 1.79–1.62 (m, 13H), 1.48–1.45 (m, 2H). ¹³C NMR (100 Hz, DMSO-*d*₆) δ (ppm) 172.2, 171.7, 53.2, 46.4, 37.7, 37.4, 35.3, 35.2, 32.0, 31.4, 28.5, 27.3, 27.2, 22.5, 20.6. ESI-HRMS: *m/z* [M+Na]⁺ calcd for C₁₉H₃₂N₂O₂Na: 343.2356; found: 343.2361.

N [1]-((5*S*,7*S*)-5-hydroxyadamantan-2-yl)-*N* [5]-isobutylglutaramide (**E303**). According to General procedure for acylation of carboxylic acids with amines. **E303** was obtained as a white solid (0.49 g, 49%). m.p. 181–183 °C. ¹H NMR (400 Hz, DMSO-*d*₆) δ (ppm) 7.74 (t, *J* = 5.5 Hz, 1H), 7.59 (d, *J* = 7.4 Hz, 1H), 4.37 (s, 1H), 3.76–3.74 (m, 1H), 2.85 (t, *J* = 6.1 Hz, 2H), 2.12 (t, *J* = 7.4 Hz, 2H), 2.06 (t, *J* = 7.4 Hz, 2H), 1.97 (br, 1H), 1.88–1.84 (m, 4H), 1.73–1.63 (m, 5H), 1.62–1.56 (m, 4H), 1.31–1.28 (m, 2H), 0.82 (d, *J* = 6.7 Hz, 6H). ¹³C NMR (100 Hz, DMSO-*d*₆) δ (ppm) 172.2, 171.9, 66.0, 52.6, 46.4, 45.8, 45.1, 35.3, 35.2, 33.8, 30.4, 29.6, 28.5, 22.4, 20.6. ESI-HRMS: *m/z* [M+Na]⁺ calcd for C₁₉H₃₂N₂O₃Na: 359.2305; found: 359.2332.

General procedure for the syntheses of compounds 21 – 23. To a solution of amines (80.8 mmol), Et₃N (16.4 g, 0.16 mol) in dry THF (25 mL) was added dropwise a solution of 4-nitrobenzoyl chloride (10.0 g, 53.9 mmol) in THF (40 mL) at 0 °C under ice bath. The reaction mixture was allowed to warm to rt and stirred for 6 h. Then solvent was evaporated, and the residues were dissolved in EtOAc (50 mL) and treated with water (40 mL). The organic layer was separated, and the water layer was extracted with EtOAc (30 mL × 3). The combined organic layers were washed twice with 1 N hydrochloric acid (30 mL), twice with water (30 mL), once with brine (30 mL), dried over MgSO₄, filtered, and concentrated to produce yellow oil. The crude product was triturated with diethyl ether to afford the title compound as a white solid.

General procedure for the syntheses of compounds 24 – 26. Nitro compounds (**21–23**) (42.7 mmol) was dissolved in EtOH (100 mL), and the solution was vacuumed briefly then put under an argon atmosphere. Then 5%Pd/C (10% w/w) was quickly added to the solution that was vacuumed and put under argon atmosphere. This was repeated three times. The solution was briefly vacuumed to remove the argon atmosphere then put under a H₂ atmosphere; this was repeated three times. The mixture was heated to 50 °C for 12 h. After the reaction mixture was cooled to rt, the reaction was filtered through a celite pad and concentrated *in vacuo* to give a white solid.

General procedure for the syntheses of compounds 27 – 29. To a solution of Compounds (**24–26**) (26.9 mmol), K₂CO₃ (40.4 mmol) in DCM (20 mL) was added dropwise a solution of phenyl chloroformate (35.3 mmol) in DCM (20 mL) at 0 °C. The reaction mixture

was allowed to warm to rt and stirred for 7 h. The reaction mixture was poured into water (40 mL), the resulting precipitation was filtered and washed with H₂O to give a crude product, which was triturated with diethyl ether to afford the title compound as a white solid.

General procedure for the syntheses of urea-based compounds.

To a solution of carbamate intermediates (compounds **27–29**) (1.54 mmol), Et₃N (3.08 mmol) in THF (5 mL) was added corresponding amines (1.70 mmol). The reaction mixture was heated to reflux for 8 h. After cooling to the rt, the resulting precipitation was filtered and washed with THF to give a little product as a white solid.

1-((1*r*,3*R*,5*S*,7*r*)-3,5-dimethyladamantan-1-yl)-3-(4-(piperidine-1-carbonyl)phenyl)urea (B401**). White solid (0.41 g, 65%). m.p. 204–205 °C. Compound **B401** used for animal experiment exhibited >99.9% purity by HPLC (Shimadzu 2010A). Purity assessment of **B401** was performed by injecting 2 μ L (2 mg/mL) of sample of interest in 1:1 MeOH onto a reverse-phase Agilent ZORBA \times 80A Extend-C18 (4.6 \times 150 mm, 5 μ m) column under the following mobile-phase conditions: MeCN/H₂O = 75%/25%. The mobile-phase flow rate was 0.8 mL/min, and the column temperature was set to 25 °C. Analytical UV detection was performed at wavelength of 210 and 230 nm. The retention time of **B401** was 4.949 min. ¹H NMR (400 Hz, CDCl₃) δ (ppm) 8.41 (s, 1H), 7.37 (d, *J* = 8.6 Hz, 2H), 7.22 (d, *J* = 8.6 Hz, 2H), 5.95 (s, 1H), 3.42 (br, 4H), 2.10–2.08 (m, 1H), 1.76–1.75 (m, 2H), 1.61–1.55 (m, 6H), 1.49 (br, 4H), 1.35–1.24 (m, 4H), 1.12 (s, 2H), 0.83 (s, 6H). ¹³C NMR (100 Hz, DMSO-*d*₆) δ (ppm) 169.5, 154.3, 142.2, 128.8, 128.3, 117.1, 52.0, 50.8, 48.1, 42.8, 40.6, 32.4, 30.5, 30.1, 26.1, 24.6. ESI-HRMS: *m/z* [M+Na]⁺ calcd for C₂₅H₃₅N₃O₂Na: 432.2621; found: 432.2646.**

N-cyclohexyl-4-(3-((1*r*,3*R*,5*S*,7*r*)-3,5-dimethyladamantan-1-yl)ureido)benzamide (B402**). White solid (0.39 g, 62%). m.p. >300 °C. ¹H NMR (400 Hz, DMSO-*d*₆) δ (ppm) 8.47 (s, 1H), 7.94 (d, *J* = 8.0 Hz, 2H), 7.71 (d, *J* = 8.7 Hz, 2H), 7.77 (d, *J* = 8.7 Hz, 2H), 5.97 (s, 1H), 3.73–3.72 (m, 1H), 2.10–2.08 (m, 1H), 1.79–1.73 (m, 6H), 1.61–1.58 (m, 5H), 1.34–1.25 (m, 8H), 1.15–1.09 (m, 3H), 0.83 (s, 6H). ¹³C NMR (100 Hz, DMSO-*d*₆) δ (ppm) 165.3, 154.2, 143.6, 128.6, 127.4, 116.6, 52.1, 50.7, 48.6, 48.1, 42.8, 40.6, 33.0, 32.4, 30.6, 30.1, 25.8, 25.5. ESI-HRMS: *m/z* [M+Na]⁺ calcd for C₂₆H₃₇N₃O₂Na: 446.2778; found: 446.2810.**

4-(3-((1*r*,3*R*,5*S*,7*r*)-3,5-dimethyladamantan-1-yl)ureido)-N-isobutylbenzamide (B403**). White solid (0.33 g, 52%). m.p. >300 °C. ¹H NMR (400 Hz, DMSO-*d*₆) δ (ppm) 8.68 (s, 1H), 8.22 (t, *J* = 5.8 Hz, 1H), 7.72 (d, *J* = 8.8 Hz, 2H), 7.38 (t, *J* = 7.1 Hz, 2H), 6.13 (s, 1H), 3.05 (t, *J* = 6.1 Hz, 2H), 2.10–2.08 (m, 1H), 1.86–1.79 (m, 1H), 1.76–1.75 (m, 2H), 1.62–1.55 (m, 4H), 1.35–1.24 (m, 4H), 1.12 (s, 2H), 0.88 (s, 3H), 0.86 (s, 3H), 0.83 (s, 6H). ¹³C NMR (100 Hz, DMSO-*d*₆) δ (ppm) 166.3, 154.3, 143.8, 128.5, 127.2, 116.6, 52.0, 50.8, 48.1, 47.1, 42.8, 40.6, 32.4, 30.5, 30.1, 28.6, 20.7. ESI-HRMS: *m/z* [M+Na]⁺ calcd for C₂₄H₃₅N₃O₂Na: 420.2661; found: 420.2655.**

1-(1-((1*s*,3*s*)-adamantan-1-yl)ethyl)-3-(4-(piperidine-1-carbonyl)phenyl)urea (C401**). White solid (0.39 g, 62%). m.p. 181–183 °C. ¹H NMR (400 Hz, DMSO-*d*₆) δ (ppm) 8.50 (s, 1H), 7.41 (d, *J* = 8.6 Hz, 2H), 6.02 (d, *J* = 9.4 Hz, 1H), 3.42–3.34 (m, 5H), 1.96 (br, 3H), 1.69–1.58 (m, 8H), 1.55–1.45 (m, 10H), 0.97 (d, *J* = 6.8 Hz, 3H). ¹³C NMR (100 Hz, DMSO-*d*₆) δ (ppm) 169.5, 155.1, 142.3, 128.8, 128.3, 117.0, 53.2, 38.5, 37.2, 36.0, 28.3, 26.1, 24.6, 15.3. ESI-HRMS: *m/z* [M+Na]⁺ calcd for C₂₅H₃₅N₃O₂Na: 432.2621; found: 432.2645.**

4-(3-(1-((1*s*,3*s*)-adamantan-1-yl)ethyl)ureido)-N-cyclohexylbenzamide (C402**). White solid (0.40 g, 64%). m.p. 280–283 °C. ¹H NMR (400 Hz, DMSO-*d*₆) δ (ppm) 8.58 (s, 1H), 7.94 (d, *J* = 7.9 Hz, 1H), 7.72 (d, *J* = 8.7 Hz, 2H), 7.41 (d, *J* = 8.8 Hz, 2H), 6.06 (d, *J* = 9.4 Hz, 1H), 3.74–3.72 (m, 1H), 3.42–3.34 (m, 1H), 2.00 (br, 3H), 1.79–1.72 (m, 4H), 1.69–1.58 (m, 7H), 1.55–1.45 (m, 6H), 1.35–1.24 (m, 4H), 0.97 (d, *J* = 6.8 Hz, 3H). ¹³C NMR (100 Hz,**

DMSO-*d*₆) δ (ppm) 165.4, 155.0, 143.7, 128.7, 127.4, 116.6, 53.2, 48.6, 38.5, 37.1, 36.0, 33.0, 28.3, 25.8, 25.5. ESI-HRMS: *m/z* [M+Na]⁺ calcd for C₂₆H₃₇N₃O₂Na: 446.2778; found: 446.2800.

4-(3-(1-((1*s*,3*s*)-adamantan-1-yl)ethyl)ureido)-N-isobutylbenzamide (C403**). White solid (0.38 g, 60%). m.p. 207–209 °C. ¹H NMR (400 Hz, DMSO-*d*₆) δ (ppm) 8.59 (s, 1H), 8.21 (t, *J* = 5.7 Hz, 1H), 7.73 (d, *J* = 8.8 Hz, 2H), 7.42 (d, *J* = 8.8 Hz, 2H), 6.08 (d, *J* = 9.3 Hz, 1H), 3.42–3.34 (m, 1H), 3.05 (t, *J* = 6.1 Hz, 2H), 1.96 (br, 3H), 1.86–1.76 (m, 1H), 1.69–1.58 (m, 6H), 1.55–1.45 (m, 6H), 0.97 (d, *J* = 6.8 Hz, 3H), 0.88 (d, *J* = 6.7 Hz, 6H). ¹³C NMR (100 Hz, DMSO-*d*₆) δ (ppm) 166.3, 155.1, 143.8, 128.5, 127.3, 116.7, 53.2, 47.1, 38.5, 37.1, 36.0, 28.6, 28.3, 20.7, 15.3. ESI-HRMS: *m/z* [M+Na]⁺ calcd for C₂₄H₃₅N₃O₂Na: 420.2621; found: 420.2647.**

1-((1*S*,2*R*,5*R*)-adamantan-2-yl)-3-(4-(piperidine-1-carbonyl)phenyl)urea (D401**). White solid (0.40 g, 68%). m.p. 265–267 °C. ¹H NMR (400 Hz, DMSO-*d*₆) δ (ppm) 8.58 (s, 1H), 7.42–7.39 (m, 2H), 7.26–7.23 (m, 2H), 6.50 (d, *J* = 8.0 Hz, 1H), 3.77 (d, *J* = 7.8 Hz, 1H), 3.43 (br, 4H), 1.87–1.74 (m, 10 H), 1.70–1.49 (m, 10H). ¹³C NMR (100 Hz, DMSO-*d*₆) δ (ppm) 169.5, 154.7, 142.2, 128.9, 128.4, 117.0, 53.3, 37.6, 37.3, 32.5, 31.7, 27.2, 27.1, 26.2, 25.6, 24.6. ESI-HRMS: *m/z* [M+Na]⁺ calcd for C₂₃H₃₁N₃O₂Na: 404.2308; found: 404.2335.**

4-(3-((1*S*,2*R*,5*R*)-adamantan-2-yl)ureido)-N-cyclohexylbenzamide (D402**). White solid (0.39 g, 66%). m.p. >300 °C. ¹H NMR (400 Hz, DMSO-*d*₆) δ (ppm) 8.67 (s, 1H), 7.94 (d, *J* = 8.0 Hz, 1H), 7.73 (d, *J* = 8.7 Hz, 2H), 7.41 (d, *J* = 8.8 Hz, 2H), 6.54 (d, *J* = 8.0 Hz, 1H), 3.78–3.72 (m, 2H), 1.87–1.71 (m, 16H), 1.62–1.55 (m, 3H), 1.34–1.24 (m, 4H), 1.15–1.10 (m, 1H). ¹³C NMR (100 Hz, DMSO-*d*₆) δ (ppm) 165.4, 154.6, 143.5, 128.7, 127.5, 116.6, 53.3, 48.6, 37.6, 37.3, 33.0, 32.5, 31.7, 27.2, 27.1, 25.8, 25.5. ESI-HRMS: *m/z* [M+Na]⁺ calcd for C₂₄H₃₃N₃O₂Na: 418.2465; found: 418.2490.**

4-(3-((1*S*,2*R*,5*R*)-adamantan-2-yl)ureido)-N-isobutylbenzamide (D403**). White solid (0.41 g, 70%). m.p. 270–272 °C. ¹H NMR (400 Hz, DMSO-*d*₆) δ (ppm) 8.88 (s, 1H), 8.22 (t, *J* = 5.7 Hz, 1H), 7.73 (d, *J* = 8.7 Hz, 2H), 7.44 (d, *J* = 8.7 Hz, 2H), 6.69 (d, *J* = 8.0 Hz, 1H), 3.78–3.77 (m, 2H), 3.05 (t, *J* = 6.2 Hz, 2H), 1.91–1.70 (m, 13H), 1.57–1.54 (m, 2H), 0.88 (d, *J* = 6.7 Hz, 6H). ¹³C NMR (100 Hz, DMSO-*d*₆) δ (ppm) 166.3, 154.7, 143.7, 128.6, 127.3, 116.6, 53.3, 47.1, 37.6, 37.3, 32.6, 31.7, 28.6, 27.2, 27.1, 20.7. ESI-HRMS: *m/z* [M+Na]⁺ calcd for C₂₂H₃₁N₃O₂Na: 392.2308; found: 392.2326.**

1-((5*S*,7*S*)-5-hydroxyadamantan-2-yl)-3-(4-(piperidine-1-carbonyl)phenyl)urea (E401**). White solid (0.42 g, 69%). m.p. 270–272 °C. ¹H NMR (400 Hz, DMSO-*d*₆) δ (ppm) 8.58 (s, 1H), 7.42 (d, *J* = 8.6 Hz, 2H), 7.25 (d, *J* = 8.6 Hz, 2H), 6.44 (d, *J* = 7.8 Hz, 1H), 4.41 (s, 1H), 3.71–3.69 (m, 1H), 3.43 (br, 4H), 2.03 (br, 1H), 1.93 (br, 2H), 1.76–1.62 (m, 10H), 1.49–1.34 (m, 6H). ¹³C NMR (100 Hz, DMSO-*d*₆) δ (ppm) 169.5, 154.7, 142.1, 129.0, 128.4, 117.0, 65.9, 52.7, 45.8, 44.9, 34.3, 30.6, 29.6, 26.1, 24.6. ESI-HRMS: *m/z* [M+Na]⁺ calcd for C₂₃H₃₁N₃O₃Na: 420.2258; found: 420.2281.**

N-cyclohexyl-4-(3-((5*S*,7*S*)-5-hydroxyadamantan-2-yl)ureido)benzamide (E402**). White solid (0.46 g, 75%). m.p. >300 °C. ¹H NMR (400 Hz, DMSO-*d*₆) δ (ppm) 8.63 (s, 1H), 7.94 (d, *J* = 7.9 Hz, 1H), 7.73 (d, *J* = 8.7 Hz, 2H), 7.41 (d, *J* = 8.7 Hz, 2H), 6.45 (d, *J* = 7.8 Hz, 1H), 4.41 (s, 1H), 3.71–3.69 (m, 2H), 2.03 (br, 1H), 1.93 (br, 2H), 1.79–1.68 (m, 8H), 1.64–1.62 (m, 5H), 1.45–1.38 (m, 2H), 1.34–1.23 (m, 4H), 1.17–1.10 (m, 1H). ¹³C NMR (100 Hz, DMSO-*d*₆) δ (ppm) 165.4, 154.6, 143.5, 128.7, 127.5, 116.6, 65.9, 52.7, 48.6, 45.8, 44.9, 34.3, 33.0, 30.6, 29.6, 25.8, 25.5. ESI-HRMS: *m/z* [M+Na]⁺ calcd for C₂₄H₃₃N₃O₃Na: 434.2414; found: 434.2437.**

4-(3-((5*S*,7*S*)-5-hydroxyadamantan-2-yl)ureido)-N-isobutylbenzamide (E403**). White solid (0.44 g, 72%). m.p. 270–272 °C. ¹H NMR (400 Hz, DMSO-*d*₆) δ (ppm) 8.65 (s, 1H), 8.22 (t, *J* = 5.6 Hz, 1H), 7.74 (d, *J* = 8.6 Hz, 2H), 7.42 (d, *J* = 8.6 Hz, 2H), 6.47 (d, *J* = 7.7 Hz, 1H), 4.42 (s, 1H), 3.72–3.70 (m, 1H), 3.05 (t, *J* = 6.3 Hz, 2H), 2.03 (br, 1H), 1.94 (br, 2H), 1.86–1.81 (m, 1H), 1.79–1.57 (m, 9H), 1.41–1.38 (m, 2H), 0.87 (d, *J* = 7.4 Hz, 6H). ¹³C NMR (100 Hz,**

DMSO- d_6) δ (ppm) 166.3, 154.6, 143.5, 128.6, 127.5, 116.7, 65.9, 52.7, 47.1, 45.8, 44.9, 34.3, 30.6, 29.6, 28.6, 25.6, 20.7. ESI-HRMS: m/z [M+Na]⁺ calcd for C₂₂H₃₁N₄O₃Na: 408.2258; found: 408.2282.

N [1]-((1*r*,3*s*,5*R*,7*S*)-3-hydroxyadamantan-1-yl)-**N** [5]-isobutylglutaramide (**F401**). White solid (0.45 g, 73%). m.p. 245–247 °C. ¹H NMR (400 Hz, DMSO- d_6) δ (ppm) 8.42 (s, 1H), 7.37 (d, J = 8.5 Hz, 2H), 7.23 (d, J = 8.6 Hz, 2H), 6.00 (s, 1H), 4.80 (s, 1H), 3.42 (br, 4H), 2.14 (br, 2H), 1.85–1.42 (m, 6H), 1.61–1.42 (m, 12H). ¹³C NMR (100 Hz, DMSO- d_6) δ (ppm) 169.5, 154.2, 142.2, 128.8, 128.3, 117.1, 67.8, 53.0, 50.1, 44.7, 41.0, 35.3, 30.6, 26.2, 24.6. ESI-HRMS: m/z [M+Na]⁺ calcd for C₂₃H₃₁N₃O₃Na: 420.2258; found: 420.2279.

N-cyclohexyl-4-(3-((1*r*,3*s*,5*R*,7*S*)-3-hydroxyadamantan-1-yl)ureido)benzamide (**F402**). White solid (0.43 g, 71%). m.p. 263–265 °C. ¹H NMR (400 Hz, DMSO- d_6) δ (ppm) 8.54 (s, 1H), 7.94 (d, J = 7.9 Hz, 1H), 7.72 (d, J = 8.8 Hz, 2H), 7.37 (d, J = 8.8 Hz, 2H), 6.08 (s, 1H), 4.48 (s, 1H), 3.74–3.72 (m, 1H), 2.14 (br, 2H), 1.85–1.77 (m, 8H), 1.73–1.72 (m, 2H), 1.61–1.51 (m, 5H), 1.47–1.42 (m, 2H), 1.35–1.24 (m, 4H), 1.13–1.10 (m, 1H). ¹³C NMR (100 Hz, DMSO- d_6) δ (ppm) 165.4, 154.1, 143.6, 128.6, 127.4, 116.6, 67.8, 53.0, 50.1, 48.6, 44.7, 41.0, 35.3, 33.0, 30.6, 25.8, 25.5. ESI-HRMS: m/z [M+Na]⁺ calcd for C₂₄H₃₃N₃O₃Na: 434.2414; found: 434.2439.

4-(3-((1*r*,3*s*,5*R*,7*S*)-3-hydroxyadamantan-1-yl)ureido)-**N**-isobutylbenzamide (**F403**). White solid (0.46 g, 74%). m.p. 156–158 °C. ¹H NMR (400 Hz, DMSO- d_6) δ (ppm) 8.48 (s, 1H), 8.22 (t, J = 5.7 Hz, 1H), 7.72 (d, J = 8.8 Hz, 2H), 7.38 (d, J = 8.8 Hz, 2H), 6.03 (s, 1H), 4.49 (s, 1H), 3.05 (t, J = 6.6 Hz, 2H), 2.14 (br, 2H), 1.85–1.76 (m, 7H), 1.57–1.42 (m, 6H), 0.87 (d, J = 6.7 Hz, 6H). ¹³C NMR (100 Hz, DMSO- d_6) δ (ppm) 166.3, 154.1, 143.6, 128.5, 127.3, 116.7, 67.8, 53.0, 50.1, 47.1, 44.7, 41.0, 35.3, 30.6, 28.6, 25.6, 20.7. ESI-HRMS: m/z [M+Na]⁺ calcd for C₂₂H₃₁N₄O₃Na: 408.2258; found: 408.2286.

4.3. In vitro biological activity assays

All HsEH and MsEH IC₅₀ values is the concentration of a compound that reduces the sEH activity by 50%. The IC₅₀ values were determined using a fluorescent-based assay [(3-phenyloxiranyl) acetic acid cyano(6-methoxynaphthalen-2-yl)methyl ester (PHOME) as the substrate] [31]. The fluorescent assay was used with purified recombinant human, or mouse sEH proteins. The enzymes were incubated at 37 °C with the inhibitors ([I]_{final} = 0.4 – 100,000 nM) for 10 min in 25 mM Tris HCl buffer (pH = 7.4) containing 0.1 mg/mL of BSA and 1% of DMSO. The substrate (PHOME) was then added ([S]_{final} = 50 μ M). Activity was assessed by measuring the formation of the fluorescent 6-methoxynaphthaldehyde product (λ_{ex} = 330 nm, λ_{em} = 465 nm) on a SpectraMax M2 (molecular devices). Results were obtained by regression analysis from a linear region of the curve.

4.4. In vivo safety

All animal experiments were performed under the guidelines of the Jiangsu Kanion Pharmaceutical Co., Ltd. Committee for Use and Care of Animals using an approved animal protocol. Mice used in this study were ICR (half females and half males, 6 – 8 weeks old, body weight 16–18 g) and purchased from Comparative Medicine Center of Yangzhou University. The animals were housed under sterile conditions at a constant temperature of 22–24 °C under daily cycles of light/darkness (12 h). After adaptive feeding three days, mice were randomly divided into vehicle group, **B401** group and AR-9281 group (n = 9 – 10). The vehicle was soybean oil, mice were administered intraperitoneal injection (*ip*) with a single dose of 100 mg/kg of test compounds. The volume of administration was 10 mL/kg. Animals were weighed before each administration to adjust the required volume. After administration of 1, 3 and 6 h, clinical symptoms and death/near death situation were observed

(including general conditions, behavioral activities, gait and posture, eyes, nose and mouth, gastrointestinal function, skin coat, urogenital tract). After that, clinical symptoms were monitored for 14 days. The animals' weight was monitored for 7 days. Statistical analysis for the body weight was performed using GraphPad Prism 6 software.

4.5. Microsomal stability

Human and SD rat hepatic microsomes were purchased from Research Institute for Liver Diseases (Shanghai, China) Co., Ltd. The incubation mixture consisted of microsomal protein in PBS buffer (100 mM, pH = 7.4) and 100 ng/mL B401 in a final volume of 100 μ L. The concentration of human hepatic microsomal protein was 0.4 mg/mL (0.53 mg/mL of SD rat). A 0.83 mg/mL NADPH solution was prepared and added to the PBS buffer. After the addition of the NADPH-generating system, the resulting mixture was incubated at 37 °C for 0, 5, 10, 20, 30 and 60 min. The reaction was terminated by the addition of methanol 300 μ L containing diphenhydramine (0.02 ng/mL). The mixture was vortexed for 1 min, centrifuged at 21,528 \times g for 10 min at 4 °C. After centrifugation, 200 μ L of the supernatant was transferred to 96-well plate, and 400 μ L of purified water was added, and the solution was mixing with shaker at 500 rpm for 5 min. The concentrations of B401 in the reaction mixture were measured by LC/MS/MS, using an AB SCIEX 4500MD mass spectrometer (Rockwell Allen-Bradley, USA).

4.6 In Vivo Pharmacokinetics (PK) study.
SD rats (6 females, 6 males, and 8 weeks old) were used in this study. All animal procedures were performed in accordance with the Guidelines for Care and Use of Laboratory Animals of Jiangsu Kanion Pharmaceutical Co., Ltd. and experiments were approved by the Animal Ethics Committee of Jiangsu Kanion Pharmaceutical Co., Ltd. 12 SD rats were randomly divided into two groups (half females and males). The 6 SD rats was administered *iv* with a single dose of 3 mg/kg of compound **B401**, and the other 6 SD rats were administered *po* with a single dose of 30 mg/kg of compound **B401**. Animals were weighed before each administration to adjust the required volume. Blood samples (*iv* group) were collected at different time: 0 min, 5 min, 15 min, 30 min, 1, 2, 4, 6, 8 and 12 h. Blood samples (*po* group) were collected at different time: 0 min, 10 min, 30 min, 1, 2, 4, 6, 8, 12 and 24 h. Blood was taken from the orbital vein. Blood was collected on Eppendorf tubes (1.5 mL) containing of EDTA, then centrifuged at 4800 rpm for 10 min. Each plasma sample (50 μ L) was mixed with 150 μ L of tolbutamide in acetonitrile (5 ng/mL) and was centrifuged at 13,000 rpm for 10 min. After that, 50 μ L of supernatant was reconstituted with 200 μ L of acetonitrile, and resulting concentrations of compound **B401** analyzed by LC-MS.

4.6. Percentage plasma protein binding (%PPB)

Compound B401 was dissolved in a 1: 19: 480 mixture of DMSO, MeCN and 0.1 M PBS, and to achieve a concentration of 0.02 mM. First, 96-well plate with 380 μ L aliquots of plasma in the wells designated for mouse plasma respectively were preloaded. Then, 20 μ L of solution (0.02 mM) was spiked into the pre-loaded plasma in the 96-well plate. The final concentration of B401 was 1 μ M, containing 0.01% DMSO. Third, aliquots of 100 μ L of control dialysis buffer were added to the receiver side of dialysis chambers. Aliquots of 100 μ L of the plasma spiking with B401 and warfarin (final concentration: 1 μ M) were added to the donor side of the dialysis chambers. Then, the dialysis block was covered with a plastic lid and placed the entire apparatus in a shaker (120 rpm) for 5 h at 37 °C. At end of incubation, each of post-dialysis samples was took out from the buffer and plasma chambers. After mixing solution

(total 300 μ L) from plasma and buffer chamber, control plasma, PBS and internal standard solution, the samples (0, 5 h) were vortexed at 600 rpm for 10 min, followed by centrifugating at 6000 rpm for 15 min. Then, 100 μ L of the supernatant from each well was transferred into 96-well plate containing 100 μ L of ultrapure water, the resulting mixture was further analyzed by LC-MS/MS. The content of compound B401 was measured by LC-MS/MS-20 (TQ-6500+) with ACQUITY UPLC HSS T3 1.8 μ m (50 mm \times 2.10 mm) column under the following mobile phase conditions: 0.01 – 0.3 min 90:10 to 5:95 A/B, 0.3 – 1 min 5:95 A/B, 1.01 – 1.5 min 90:10, where A = 0.1% formic acid in water and B = 0.1% formic acid in MeCN. The mobile phase flow rate was 0.6 mL/min. The %PPB value of the compound was calculated by following equation: % PPB = $100 \times ([\text{Donor}]_{5h} - [\text{Receiver}]_{5h}) / [\text{Donor}]_{5h}$. The experimental system was calibrated using the standard compound warfarin of known %PPB: mouse plasma (94.6%).

4.7 In Vivo Efficacy of B401.

All animal experiments were performed under the guidelines of the Jiangsu Kanion Pharmaceutical Co., Ltd. Committee for Use and Care of Animals using an approved animal protocol. Mice used in this study were C57BL/6 (females, body weight 14 – 16 g) and purchased from Comparative Medicine Center of Yangzhou University. The animals were housed under sterile conditions at a constant temperature of 22–24 °C under daily cycles of light/darkness (12 h). After adaptive feeding seven days, 70 C57BL/6 mice were randomly divided into five groups (soybean oil vehicle, **B401** three doses groups, dexamethasone group). The mice were fasted for 6–8 h and freely drinking water before the experiment. Mice were administered *ip* with LPS (30 mg/kg), then dosed by *ip* with either vehicle or **B401** at 1, 5, 20 mg/kg, administered at 0, 8 and 24 h intervals. Survival rate of mice was observed and record for 72 h. The survival curve was analyzed by log-rank (Mantel-Cox) test of GraphPad Prism software.

Funding sources

This work was funded by the Liaoning Revitalization Talents Program (XLYC1908031), Basic Research Project of Department of Education of Liaoning Province – natural sciences (2020LJC02), and partial support was provided by the NIH – NIEHS (RIVER Award) R35 ES030443-01, the NIEHS Superfund Research Program P42 ES004699.

Declaration of competing interest

The authors declare that they have no known competing financial interests or personal relationships that could have appeared to influence the work reported in this paper.

Appendix A. Supplementary data

Supplementary data to this article can be found online at <https://doi.org/10.1016/j.ejmech.2021.113678>.

References

- W. Cho, J.Y. Koo, Y. Park, K. Oh, S. Lee, J.S. Song, M.A. Bae, D. Lim, D.S. Lee, S.B. Park, Treatment of sepsis pathogenesis with high mobility group box protein 1-regulating anti-inflammatory agents, *J. Med. Chem.* 60 (2017) 170–179.
- C. Fleischmann, C.A. Scherag, N.K. Adhikari, C.S. Hartog, T. Tsaganos, P. Schlattmann, D.C. Angus, K. Reinhart, Assessment of global incidence and mortality of hospital-treated sepsis. current estimates and limitations, *Am. J. Respir. Crit. Care Med.* 193 (2016) 259–272.
- C.M. Torio, R.M. Andrews, National Inpatient Hospital Costs: the Most Expensive Conditions by Payer, 2011; U.S. agency for health care policy and research, Rockville, MD, 2013.
- D.C. Angus, T. van der Poll, Severe sepsis and septic shock, *N. Engl. J. Med.* 369 (2013) 840–851.
- R. Pukkila-Worley, R. Feinbaum, N.V. Kirienko, J. LarkinsFord, A.L. Conery, F.M. Ausubel, Stimulation of host immune defenses by a small molecule protects *C. elegans* from bacterial infection, *PLoS Genet.* 8 (2012) e1002733–e1002744.
- S.F. Pedersen, Y.C. Ho, Sars-CoV-2, A storm is raging, *J. Clin. Invest.* 130 (2020) 2202–2205.
- P. Conti, G. Ronconi, A. Caraffa, C.E. Gallenga, R. Ross, I. Frydas, S.K. Kritas, Induction of pro-inflammatory cytokines (IL-1 and IL-6) and lung inflammation by Coronavirus-19 (COVID-19 or SARS-CoV-2): anti-inflammatory strategies, *J. Biol. Regul. Homeost. Agents* 34 (2020) 327–331.
- P. Mehta, D.F. McAuley, M. Brown, E. Sanchez, R.S. Tattersall, J.J. Manson, COVID-19: consider cytokine storm syndromes and immunosuppression, *Lancet* 395 (2020) 1033–1034.
- M. Rodriguez, M. Clare-Salzler, Eicosanoid imbalance in the NOD mouse is related to a dysregulation in soluble epoxide hydrolase and 15-PGDH expression, *Ann. N. Y. Acad. Sci.* 1079 (2006) 130–134.
- A. Gartung, J. Yang, V.P. Sukhatme, D.R. Bielenberg, D. Fernandes, J. Chang, B.A. Schmidt, S.H. Hwang, D. Zurakowski, S. Huang, M.W. Kieran, B.D. Hammock, D. Panigrahy, Suppression of chemotherapy-induced cytokine/lipid mediator surge and ovarian cancer by a dual COX-2/sEH inhibitor, *Proc. Natl. Acad. Sci. U. S. A.* 116 (2019) 1698–1703.
- K.R. Schmelzer, L. Kubala, J.W. Newman, I.H. Kim, J.P. Eiserich, B.D. Hammock, Soluble epoxide hydrolase is a therapeutic target for acute inflammation, *Proc. Natl. Acad. Sci. U.S.A.* 102 (2005) 9772–9777.
- L. Calzetta, M. Aiello, A. Frizzelli, P. Rogliani, A. Chetta, Dexamethasone in patients hospitalized with COVID-19: whether, when and to whom, *J. Clin. Med.* 10 (2021) 1607–1613.
- B.M. Tomazini, I.S. Maia, A.B. Cavalcanti, O. Berwanger, R.G. Rosa, V.C. Veiga, A. Avezum, R.D. Lopes, F.R. Bueno, M.V.A.O. Silva, F.P. Baldassare, E.L.V. Costa, R.A.B. Moura, M.O. Honorato, A.N. Costa, L.P. Damiani, T. Lisboa, L. Kawano-Dourado, F.G. Zampieri, G.B. Olivato, C. Rigby, C.P. Amendola, R.M.L. Roepke, D.H.M. Freitas, D.N. Forte, F.G.R. Freitas, C.C.F. Fernandes, L.M.G. Melro, G.F.S. Junior, D.C. Morais, S. Zung, F.R. Machado, L.C.P. Azevedo, Effect of dexamethasone on days alive and ventilator-free in patients with moderate or severe acute respiratory distress syndrome and COVID-19 the codex randomized clinical trial, *JAMA, J. Am. Med. Assoc.* 324 (2020) 1307–1316.
- J.D. Imig, B.D. Hammock, Soluble epoxide hydrolase as a therapeutic target for cardiovascular diseases, *Nat. Rev. Drug Discov.* 8 (2009) 794–805.
- C. Morisseau, B.D. Hammock, Impact of soluble epoxide hydrolase and epoxyeicosanoids on human health, *Annu. Rev. Pharmacol. Toxicol.* 53 (2013) 37–58.
- N. Chiamvimonvat, C.M. Ho, H.J. Tsai, B.D. Hammock, The soluble epoxide hydrolase as a pharmaceutical target for hypertension, *J. Cardiovasc. Pharmacol.* 50 (2007) 225–237.
- C. Morin, M. Sirois, V. Echave, M.M. Gomes, E. Rousseau, 14,15-EET displays anti-inflammatory effects in TNF α -stimulated human bronchi: putative role of CPI-17, *Am. J. Respir. Cell Mol. Biol.* 38 (2008) 192–201.
- K.M. Wagner, A. Gomes, C.B. Reynolds, B.D. Hammock, Soluble epoxide hydrolase regulation of lipid mediators limits pain, *Neurotherapeutics* 17 (2020) 900–916.
- B. Inceoglu, A. Betteieb, C.A. Trindade da Silva, K.S. Lee, F.G. Haj, B.D. Hammock, Endoplasmic reticulum stress in the peripheral nervous system is a significant driver of neuropathic pain, *Proc. Natl. Acad. Sci. U.S.A.* 112 (2015) 9082–9087.
- R. Blöcher, K.M. Wagner, R.R. Gopireddy, T.R. Harris, H. Wu, B. Barnych, S.H. Hwang, Y.K. Xiang, E. Proschak, C. Morisseau, B.D. Hammock, Orally available soluble epoxide hydrolase/phosphodiesterase 4 dual inhibitor treats inflammatory pain, *J. Med. Chem.* 61 (2018) 3541–3550.
- E. Ono, S. Dutile, S. Kazani, M.E. Wechsler, B.D. Yang, J. Hammock, D.N. Doua, Y. Tabet, R. Khaddaj-Mallat, M. Sirois, C. Sirois, E. Rizcallah, E. Rousseau, R. Martin, E.R. Sutherland, M. Castro, N.N. Jarjour, E. Israel, B.D. Levy, Lipoxin generation is related to soluble epoxide hydrolase activity in severe asthma, *Am. J. Respir. Crit. Care Med.* 190 (2014) 886–897.
- D. Chen, R. Whitcomb, E. MacIntyre, V. Tran, Z.N. Do, J. Sabry, D.V. Patel, S.K. Anandan, R. Gless, H.K. Webb, Pharmacokinetics and pharmacodynamics of AR9281, an inhibitor of soluble epoxide hydrolase, in single- and multiple-dose studies in healthy human subjects, *J. Clin. Pharmacol.* 52 (2012) 319–328.
- A.L. Lazaar, L. Yang, R.L. Boardley, N.S. Goyal, J. Robertson, S.J. Baldwin, D.E. Newby, I.B. Wilkinson, R. Tal-Singer, R.J. Mayer, J. Cheriyan, Pharmacokinetics, pharmacodynamics and adverse event profile of GSK2256294, a novel soluble epoxide hydrolase inhibitor, *Br. J. Clin. Pharmacol.* 81 (2016) 971–979.
- K.S.S. Lee, J.C. Ng, J. Yang, S.H. Hwang, C. Morisseau, K. Wagner, B.D. Hammock, Preparation and evaluation of soluble epoxide hydrolase inhibitors with improved physical properties and potencies for treating diabetic neuropathic pain, *Bioorg. Med. Chem.* 28 (2020) 115735–115746.
- B.D. Hammock, W. Wang, M.M. Gilligan, D. Panigrahy, Eicosanoids: the overlooked storm in coronavirus disease 2019 (COVID-19)? *Am. J. Pathol.* 190 (2020) 1782–1788.
- H.C. Shen, B.D. Hammock, Discovery of inhibitors of soluble epoxide hydrolase: a target with multiple potential therapeutic indications, *J. Med. Chem.* 55 (2012) 1789–1808.

- [27] S. Codony, E. Pujol, J. Pizarro, F. Feixas, E. Valverde, M.I. Loza, J.M. Brea, E. Saez, J. Oyarzabal, A. Pineda-Lucena, B. Pérez, C. Pérez, M.I. Rodríguez-Franco, R. Leiva, S. Osuna, C. Morisseau, B.D. Hammock, M. Vázquez-Carrera, S. Vázquez, 2-Oxaadamant-1-yl ureas as soluble epoxide hydrolase inhibitors: in vivo evaluation in a murine model of acute pancreatitis, *J. Med. Chem.* 63 (2020) 9237–9257.
- [28] Z. Liu, C. Sun, J. Xu, C. Morisseau, B.D. Hammock, F. Qiu, Phytochemical constituents from *Scutellaria baicalensis* in soluble epoxide hydrolase inhibition: kinetics and interaction mechanism merged with simulations, *Int. J. Biol. Macromol.* 133 (2019) 1187–1193.
- [29] C. Sun, J. Zhang, W. Zhao, J. Yi, J. Yan, Y. Wang, C. Morisseau, Z. Liu, B.D. Hammock, X. Ma, Protostane-type triterpenoids as natural soluble epoxide hydrolase inhibitors: inhibition potentials and molecular dynamics, *Bioorg. Chem.* 96 (2020) 103637–103645.
- [30] T. Moritoyo, T. Hasunuma, K. Harada, T. Tateishi, M. Watanabe, T. Kotegawa, M. Nagai, Y. Kumagai, T. Fujitani, T. Okura, T. Fukuoka, K. Miyoshi, B. Matsuura, S. Furukawa, T. Kabori, H. Moritoyo, N. Nishikawa, T. Tsujii, H. Iwaki, M. Nakamura, S. Makino, K. Ohnuma, K. Yuji, M. Hashimoto, M. Takasu, Y. Hashizume, K. You, T. Matsumura, Y. Tanaka, N. Matsumoto, J. Nakamura, J. Miura, T. Akizawa, K. Kitazawa, T. Shibata, A. Kuroki, H. Honda, M. Mukai, K. Ohashi, T. Morimoto, H. Imai, T. Okudaira, F. Sato, J. Imanaga, K. Tanaka, M. Nomoto, Effect of renal impairment on the pharmacokinetics of memantine, *J. Pharmacol. Sci.* 119 (2012) 324–329.
- [31] N.M. Wolf, C. Morisseau, P.D. Jones, B. Hock, B.D. Hammock, Development of a high-throughput screen for soluble epoxide hydrolase inhibition, *Anal. Biochem.* 355 (2006) 71–80.
- [32] P. Leeson, B. Springthorpe, The influence of drug-like concepts on decision-making in medicinal chemistry, *Nat. Rev. Drug Discov.* 6 (2007) 881–890.
- [33] A. Daina, O. Michielin, V. Zoete, SwissADME: a free web tool to evaluate pharmacokinetics, drug-likeness and medicinal chemistry friendliness of small molecules, *Sci. Rep.* 7 (2017) 42717.
- [34] M.P. Edwards, D.A. Price, Role of physicochemical properties and ligand lipophilicity efficiency in addressing drug safety risks, *Annu. Rep. Med. Chem.* 45 (2010) 380–391.